

SINGULAR PERTURBATION ANALYSIS OF A REGULARIZED MEMS MODEL*

ANNALISA IUORIO[†], NIKOLA POPOVIC[‡], AND PETER SZMOLYAN[§]

Abstract. Micro-Electro Mechanical Systems (MEMS) are defined as very small structures that combine electrical and mechanical components on a common substrate. Here, the electrostatic-elastic case is considered, where an elastic membrane is allowed to deflect above a ground plate under the action of an electric potential, whose strength is proportional to a parameter λ . Such devices are commonly described by a parabolic partial differential equation that contains a singular nonlinear source term. The singularity in that term corresponds to the so-called “touchdown” phenomenon, where the membrane establishes contact with the ground plate. Touchdown is known to imply the non-existence of steady state solutions and blow-up of solutions in finite time.

We study a recently proposed extension of that canonical model, where such singularities are avoided due to the introduction of a regularizing term involving a small “regularization” parameter ε . Methods from dynamical systems and geometric singular perturbation theory, in particular the desingularization technique known as “blow-up”, allow for a precise description of steady-state solutions of the regularized model, as well as for a detailed resolution of the resulting bifurcation diagram. The interplay between the two main model parameters ε and λ is emphasized; in particular, the focus is on the singular limit as both parameters tend to zero.

Key words. Micro-Electro Mechanical Systems, touchdown, boundary value problem, regularization, bifurcation diagram, saddle-node bifurcation, geometric singular perturbation theory, blow-up method

AMS subject classifications. 34B16, 34C23, 34E05, 34E15, 34L30, 35K67, 74G10

1. Introduction. Micro-Electro Mechanical Systems (MEMS) are very small structures that combine electrical and mechanical components on a common substrate to perform various tasks. In particular, electrostatic-elastic devices have found important applications in drug delivery [28], micro pumps [8], optics [1], and micro-scale actuators [29]. In these devices, an elastic membrane is allowed to deflect above a ground plate under the action of an electric potential V , where the distance between plate and membrane is typically much smaller than their diameter; see Figure 1. When a critical voltage threshold V^* (“pull-in voltage”) is reached, a phenomenon called *touchdown* or *snap-through* can occur, *i.e.*, the membrane touches the ground plate, which may cause a short circuit.

The physical forces acting between the elastic components of the device – which can, *e.g.*, be of Casimir or Van der Waals type – may lead to *stiction*, which causes complications in reverting the process in order to return to the original state. In the canonical mathematical models proposed in the literature [6, 17, 23, 24], such systems are described by partial differential equations involving the Laplacian or the bi-Laplacian and a singular source term. The touchdown phenomenon leads to non-existence of steady states, or blow-up of solutions in finite time, or both. Hence, no

*

Funding: This work was funded by the Fonds zur Förderung der wissenschaftlichen Forschung (FWF) via the doctoral school “Dissipation and Dispersion in Nonlinear PDEs” (project number W1245).

[†]Institute for Analysis and Scientific Computing, Vienna University of Technology, Austria (annalisa.iuorio@tuwien.ac.at).

[‡]School of Mathematics and Maxwell Institute for Mathematical Sciences, University of Edinburgh, United Kingdom (nikola.popovic@ed.ac.uk, <http://www.maths.ed.ac.uk/~npopovic/>).

[§]Institute for Analysis and Scientific Computing, Vienna University of Technology, Austria (peter.szmolyan@tuwien.ac.at).

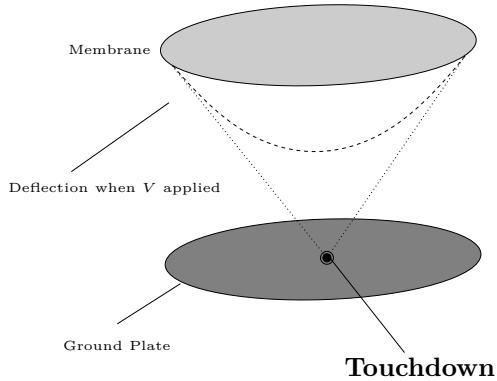


FIGURE 1. Schematic representation of an electrostatic-elastic MEMS device. The elastic membrane deflects towards the ground plate when an electric potential V is applied (dashed curve). If V exceeds a critical value V^* (the so-called “pull-in voltage”), the membrane touches the ground plate, causing touchdown (dotted line).

information on post-touchdown configurations can be captured by these models.

Recently, an extension of the canonical model has been proposed, where the introduction of a potential mimicking the effect of a thin insulating layer above the ground plate prevents physical contact between the elastic membrane and the substrate [19]. Mathematically, this corresponds to the addition of a nonlinear source term to the partial differential equation that depends on a small “regularization” parameter ε . The resulting regularized models have been studied in relevant work by Lindsay *et al.*; see *e.g.* [19, 21] for the membrane case, while the case where the elastic structure is modelled as a beam is discussed in [18, 19, 21]. In one spatial dimension, the governing equations are given by

$$(1.1) \quad u_t = u_{xx} - \frac{\lambda}{(1+u)^2} + \frac{\lambda\varepsilon^{m-2}}{(1+u)^m}$$

for $x \in [-1, 1]$, with $u = 0$ when $x = \mp 1$ (membrane)

and

$$(1.2) \quad u_t = -u_{xxxx} - \frac{\lambda}{(1+u)^2} + \frac{\lambda\varepsilon^{m-2}}{(1+u)^m}$$

for $x \in [-1, 1]$, with $u = \partial_n u = 0$ when $x = \mp 1$ (beam),

respectively. Physically speaking, the variable u denotes the (dimensionless) deflection of the surface, while the parameter λ is proportional to the square of the applied voltage V . The regularizing term $\lambda\varepsilon^{m-2}(1+u)^{-m}$ with $\varepsilon > 0$ and $m > 2$, as introduced in [19], accounts for various physical effects that are of particular relevance in the proximity of the ground plate, *i.e.*, at $u = -1$; that term induces a potential which simulates the effect of an insulating layer whose non-dimensional width is proportional to ε . In the following, we will consider $m = 4$, which corresponds to a Casimir effect; alternative choices describe other physical phenomena and can be studied in a similar fashion.

Here, we focus on steady-state solutions of the Laplacian case corresponding to a

membrane; see Equation (1.1):

$$(1.3) \quad u_{xx} = \frac{\lambda}{(1+u)^2} \left[1 - \frac{\varepsilon^2}{(1+u)^2} \right], \quad \text{for } x \in [-1, 1], \text{ with } u = 0 \text{ when } x = \mp 1.$$

For literature on the bi-Laplacian case, Equation (1.2), we refer to [19, 20, 21].

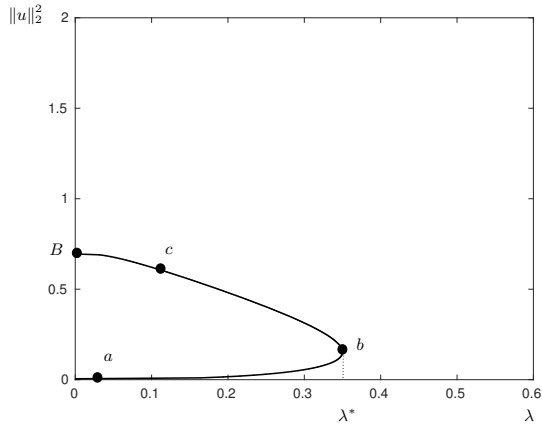
Remark 1.1. Due to the symmetry of the boundary value problem (1.3) under the transformation $x \mapsto -x$, all solutions thereof must be even; the proof is straightforward, and is omitted here.

Before addressing the novel features of the regularized model which are the focus of the present article, we briefly summarize the main properties of the non-regularized case corresponding to $\varepsilon = 0$ in (1.3), which are well understood [23, 24]. The bifurcation diagram associated to (1.3) with $\varepsilon = 0$ shown in Figure 2(a) consists of two branches of steady-state solutions, where the lower branch is stable and the upper one is unstable. The upper branch limits on the $\|u\|_2^2$ -axis in the point $B = (0, \frac{2}{3})$, which plays a crucial role in the bifurcation diagram of the regularized problem. The two branches are separated by a fold point that is located at $\lambda = \lambda^*$. For $\lambda > \lambda^*$, steady-state solutions of (1.1) cease to exist, with the transient dynamics leading to a blow-up in finite time. Sample solutions along the two branches are plotted in Figure 2(b); in addition, the piecewise linear singular solution corresponding to the point B is shown. That singular solution undergoes touchdown at $x = 0$.

The inclusion of the ε -dependent regularizing term, where $0 < \varepsilon \ll 1$, considerably alters the structure of the bifurcation diagram in Figure 2(a). The principal new feature is the emergence of a third branch of stable steady-state solutions, resulting in the S -shaped curve shown in Figure 3(a). In addition to the fact that the fold point at λ^* now depends on ε , there exists another fold point at λ_* – which is also ε -dependent – such that, for $\lambda_* < \lambda < \lambda^*$, there are three branches of steady states, the middle one of which is unstable [19]. Solutions on that newly emergent branch are in fact bounded below by $u = -1 + \varepsilon$. With increasing λ , solutions exhibit a growing “flat” portion close to $u = -1 + \varepsilon$; cf. the solution labeled d in Figure 3(b). For $\lambda < \lambda_*$ and $\lambda > \lambda^*$, there exists a unique stable steady state; in particular, and in contrast to the non-regularized case, numerical simulations indicate that a stable steady state exists for every value of $\lambda > 0$.

Remark 1.2. Figures 2 and 3 show results of numerical simulations, reproducing those presented in [19].

For very small values of ε , the bifurcation diagram in Figure 3(a) is difficult to resolve, even numerically. The highly singular nature of that diagram, as well as the influence of the regularization parameter ε on the structure thereof, are the principal features of interest to us here. Our detailed asymptotic resolution of Figure 3(a), both in the singular limit of $\varepsilon = 0$ and for ε positive and sufficiently small, is accomplished through separate investigation of three distinct, yet overlapping, regions in the diagram. To that end, we first reformulate the boundary value problem (1.3) in a dynamical systems framework; then, identification of two main parameters in the resulting equations yields a two-parameter singular perturbation problem. Careful asymptotic analysis of that problem will allow us to identify the corresponding limiting solutions, and to show how the third branch in the diagram found for non-zero ε emerges from the singular limit of $\varepsilon = 0$. On that basis, we will prove the existence and uniqueness of solutions close to these limiting solutions. While the three regions in the diagram share some common features, they need to be investigated separately



(a) Bifurcation diagram.

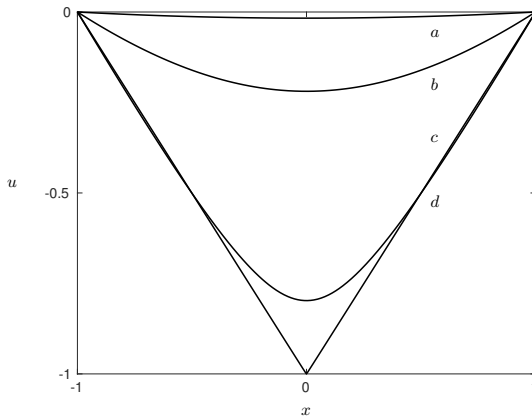
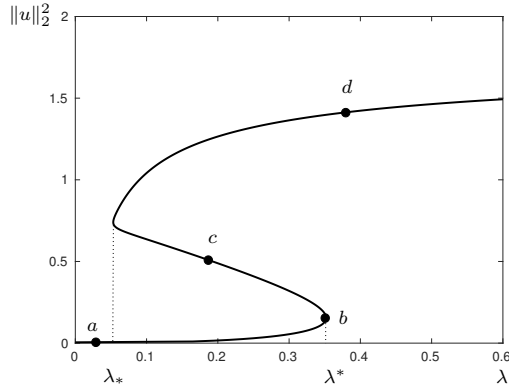
(b) Solutions in (x, u) -space.

FIGURE 2. (a) Bifurcation diagram of the membrane model, Equation (1.3), for $\varepsilon = 0$. The lower and upper branch consist of stable and unstable steady-state solutions, respectively. The solution labeled by d corresponds to the point B and represents the singular solution for $\lambda = 0$. (b) Corresponding solutions in (x, u) -space.

for the structure of the diagram to be fully resolved.

Our analysis is based on a variety of dynamical systems techniques and, principally, on geometric singular perturbation theory [5, 9, 14] and the blow-up method, or “geometric desingularization” [3, 4, 12]. In particular, a combination of these techniques will allow us to perform a detailed study of the saddle-node bifurcation at the fold point at λ_* , and to obtain an asymptotic expansion for λ_* in ε . While such an expansion has been derived by Lindsay via the method of matched asymptotic expansions [19], cf. Figure 12 therein, as well as our Figure 3(a), the leading-order coefficients in that expansion are calculated explicitly here. In the process, it is shown that the occurrence of logarithmic switchback terms in the steady-state asymptotics



(a) Bifurcation diagram.

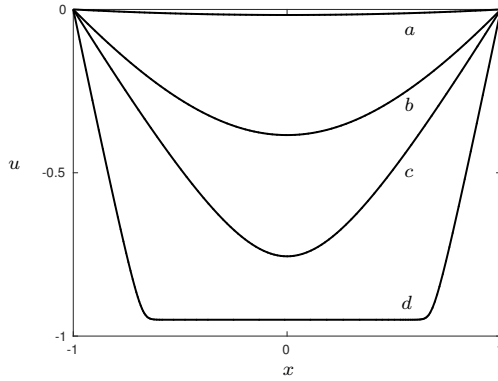
(b) Solutions in (x, u) -space.

FIGURE 3. (a) Numerically computed bifurcation diagram of the one-dimensional membrane model, Equation (1.3), for $\varepsilon = 0.05$. (b) Corresponding solutions in (x, u) -space.

for Equation (1.3), which has also been observed via asymptotic matching in [19], is due to a resonance phenomenon in one of the coordinate charts after blow-up [25]; cf. Remark 4.11.

In summary, our principal result can be expressed as follows.

THEOREM 1.3. *For $\varepsilon \in (0, \varepsilon_0)$, with $\varepsilon_0 > 0$ sufficiently small, and $\lambda \in [0, \Lambda]$, with $\Lambda = \mathcal{O}(1)$ positive and fixed, the bifurcation diagram for the boundary value problem (1.3) is as illustrated in Figure 3(a).*

Without loss of generality, we fix $\Lambda = 1$ here. The proof of Theorem 1.3 follows from a combination of Propositions 4.5, 4.16, and 4.20 below; each of these pertains to one of the three above-mentioned regions in the bifurcation diagram.

The article is structured as follows: in Section 2, we reformulate the boundary value problem (1.3) as a dynamical system. In Section 3, we introduce the principal blow-up transformation on which our analysis of the dynamics of (1.3) close to

touchdown is based. In [Section 4](#), we describe in detail the structure of the bifurcation diagram in [Figure 3\(a\)](#) by investigating separately three main regions therein, as illustrated in [Figure 9](#) below. Finally, in [Section 5](#), we discuss our findings, and we present an outlook to future research.

2. Dynamical Systems Formulation. For our analysis, we reformulate [Equation \(1.3\)](#) as a boundary value problem for a corresponding first-order system by introducing the new variable $w = u'$; here, it is useful to keep in mind that w represents the slope of the solution u to [Equation \(1.3\)](#). Moreover, we append the trivial dynamics of both the spatial variable x , which we relabel as ξ , and the regularizing parameter ε , to the resulting system:

$$\begin{aligned} (2.1a) \quad & u' = w, \\ (2.1b) \quad & w' = \frac{\lambda}{(1+u)^2} \left[1 - \frac{\varepsilon^2}{(1+u)^2} \right], \\ (2.1c) \quad & \xi' = 1, \\ (2.1d) \quad & \varepsilon' = 0; \end{aligned}$$

here, the prime denotes differentiation with respect to x . Next, we multiply the right-hand sides in [Equation \(2.1\)](#) with a factor of $(1+u)^4$, which allows us to desingularize the flow near the touchdown singularity at $u = -1$ ¹. Finally, we define a shift in u via $\tilde{u} = 1 + u$, which translates that singularity to $\tilde{u} = 0$.

Omitting the tilde and denoting differentiation with respect to the new independent variable by a prime, as before, we obtain the system

$$\begin{aligned} (2.2a) \quad & u' = u^4 w, \\ (2.2b) \quad & w' = \lambda(u^2 - \varepsilon^2), \\ (2.2c) \quad & \xi' = u^4, \\ (2.2d) \quad & \varepsilon' = 0 \end{aligned}$$

in (u, w, ξ, ε) -space, with parameter λ and subject to the boundary conditions

$$(2.3) \quad u = 1 \quad \text{for } \xi = \mp 1.$$

Since $\varepsilon \ll 1$, it seems natural to attempt a perturbative construction of solutions to the boundary value problem [\(2.2\)–\(2.3\)](#), which turns out to be non-trivial in spite of the apparent simplicity of the governing equations. For $\varepsilon = 0$, [Equation \(2.2\)](#) can be solved explicitly and admits degenerate equilibria at $u = 0$, which corresponds to the touchdown singularity at $u = -1$ in the original model, [Equation \(1.3\)](#). We denote the resulting manifold of equilibria for [\(2.2\)](#) as

$$(2.4) \quad \mathcal{S}^0 = \{(0, w, \xi, 0) \mid w \in \mathbb{R}, \xi \in \mathbb{R}\}.$$

One complication is introduced by the fact that, for $\lambda \neq 0$, the singular flow of [\(2.2\)](#) in (u, w) -space that is obtained for $\varepsilon = 0$ is not transverse to \mathcal{S}^0 ; cf. [Figure 4](#). As transversality is a necessary requirement of geometric singular perturbation theory [[5](#), [14](#)], we need to find a way to remedy the lack thereof.

¹That desingularization corresponds to a transformation of the independent variable which leaves the phase portrait of [\(2.1\)](#) unchanged for $u > -1$, since the factor $(1+u)^4$ is positive throughout then.

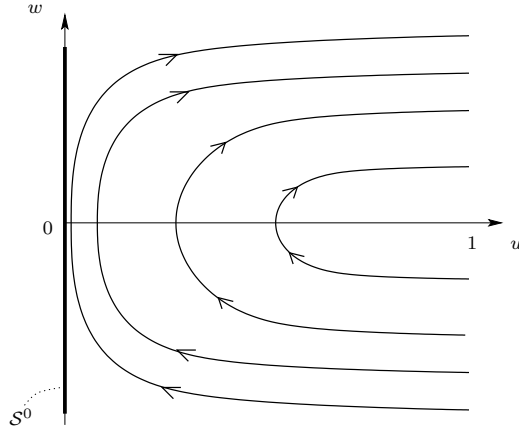


FIGURE 4. Projection of the singular flow for Equation (2.2) into (u, w) -space for $\varepsilon = 0$ and $\lambda \neq 0$. The solid black line represents the invariant manifold \mathcal{S}^0 defined in (2.4). In view of the boundary conditions in (2.3), solutions that originate and terminate at $u = 1$ are shown. All such solutions stay to the right of the manifold \mathcal{S}^0 ; those with large initial w -value tend arbitrarily close to \mathcal{S}^0 without ever reaching it. Hence, the singular flow is not transverse to \mathcal{S}^0 .

For $\lambda = 0$ in (2.2), the singular flow becomes even more degenerate; see Figure 5. Furthermore, the set

$$(2.5) \quad \mathcal{M}^0 := \{(u, 0, \xi, 0) \mid u \in \mathbb{R}^+, \xi \in \mathbb{R}\}$$

now also represents a manifold of equilibria for Equations (2.2a) and (2.2b).

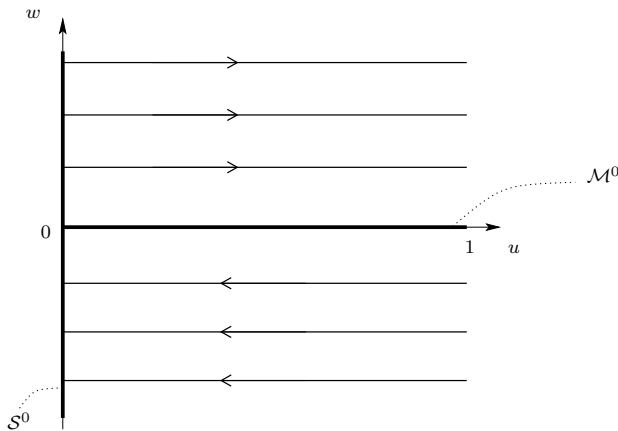


FIGURE 5. Singular flow for Equation (2.2) in (u, w) -space for $\lambda = 0$. Solid black lines represent the invariant manifolds \mathcal{S}^0 and \mathcal{M}^0 that are defined in (2.4) and (2.5), respectively. Orbits with $w \neq 0$ in (u, w) -space are now transverse to \mathcal{S}^0 ; for $w < 0$, these orbits tend towards \mathcal{S}^0 , whereas they tend away from \mathcal{S}^0 for $w > 0$. All equilibria on \mathcal{S}^0 are non-hyperbolic, as the corresponding linearization of the (u, w) -subsystem (2.2a)–(2.2b) has a double zero eigenvalue.

As it turns out, it is beneficial to introduce the following rescaling of w first:

$$(2.6) \quad w = \frac{\tilde{w}}{\delta},$$

where

$$(2.7) \quad \delta = \sqrt{\frac{\varepsilon}{\lambda}}$$

is a new, non-negative parameter.

Remark 2.1. The scaling of w by $\sqrt{\lambda}$ in (2.6) shifts λ from (2.2b) to (2.2c), the ξ -equation, after a rescaling of time. The scaling with $\varepsilon^{-\frac{1}{2}}$ in (2.6) reflects the fact that, for $\lambda = \mathcal{O}(1)$, $w = \mathcal{O}(\varepsilon^{-\frac{1}{2}})$, in agreement with numerical simulation and asymptotic analysis performed in [19].

Remark 2.2. Some parts of our analysis are conveniently carried out in the parameters ε and λ , while others are naturally described in terms of ε and δ . Hence, we will alternate between these two descriptions, as needed.

Substituting (2.6) into (2.2), multiplying the right-hand sides in the resulting equations with a factor of δ , omitting the tilde and retaining the prime for differentiation with respect to the new independent variable, as before, we find

$$(2.8a) \quad u' = u^4 w,$$

$$(2.8b) \quad w' = \varepsilon(u^2 - \varepsilon^2),$$

$$(2.8c) \quad \xi' = \delta u^4,$$

$$(2.8d) \quad \varepsilon' = 0,$$

still subject to the boundary conditions

$$(2.9) \quad u = 1 \quad \text{for } \xi = \mp 1.$$

We remark that the fast-slow structure of Equation (2.8) is very simple, since Equations (2.8a) and (2.8b) decouple from Equation (2.8c); the latter induces a slow drift in ξ .

Equations (2.8) and (2.9) will form the basis for the subsequent analysis. Two strategies suggest themselves for constructing solutions to the boundary value problem (2.8)–(2.9). The first such strategy involves two sets of boundary conditions, corresponding to suitable intervals of w -values that are defined at $\xi = -1$ and $\xi = 1$, respectively. Flowing these two sets of boundary conditions forward and backward, respectively, we verify the transversality of the intersection of the two resulting manifolds at $\xi = 0$. Each initial w -value w_0 for which these two manifolds intersect gives a solution to the boundary value problem (2.8)–(2.9).

Since all such solutions are even, by Remark 1.1, another possible strategy consists of considering Equation (2.8) on the ξ -interval $[-1, 0]$, with boundary conditions $u(-1) = 1$ and $w(0) = 0$. The set of initial conditions at $\xi = -1$ and $u = 1$, but with arbitrary initial w -value w_0 , is then tracked forward up to the hyperplane $\{w = 0\}$. The resulting manifold is naturally parametrized by $u(w, \varepsilon, \delta, w_0)$ and $\xi(w, \varepsilon, \delta, w_0)$; the unique “correct” value $w_0(\varepsilon, \delta)$ corresponding to a solution to the boundary value problem (2.8)–(2.9) is then obtained by solving $\xi(w_0, \varepsilon, \delta) = 0$ under the constraint that $w(w_0, \varepsilon, \delta) = 0$. Details will be presented in the individual proofs below. Given Remark 1.1, any solution can be obtained via that second strategy; in fact, the intrinsic symmetry of the problem is also clearly visible in Figure 3(b).

Equation (2.8) constitutes a two-parameter fast-slow system in its fast formulation. The small parameter ε represents the principal singular perturbation parameter

here, while the limit of $\delta \rightarrow 0$ is also singular. For $\delta = \mathcal{O}(1)$, the variables u and ξ are fast, while w is slow; however, for δ small, the variable ξ is slow, as well. The manifold \mathcal{S}^0 defined in (2.4) is still invariant under the flow of (2.8). Furthermore, for $\delta = 0$, the manifold \mathcal{M}^0 defined in (2.5) also represents a set of equilibria for (2.8). (We remark that the same scenario occurs for $\lambda = 0$ in (2.2).)

Setting $\varepsilon = 0$ in Equation (2.8), we obtain the so-called *layer problem*

$$(2.10a) \quad u' = u^4 w,$$

$$(2.10b) \quad w' = 0,$$

$$(2.10c) \quad \xi' = \delta u^4,$$

$$(2.10d) \quad \varepsilon' = 0;$$

see Figure 5 for an illustration of the corresponding phase portrait in (u, w) -space and, in particular, of the transversality of orbits of the layer problem to \mathcal{S}^0 . Rescaling the independent variable in (2.8) by multiplying it with ε yields the slow formulation

$$(2.11a) \quad \varepsilon \dot{u} = u^4 w,$$

$$(2.11b) \quad \dot{w} = u^2 - \varepsilon^2,$$

$$(2.11c) \quad \varepsilon \dot{\xi} = \delta u^4,$$

$$(2.11d) \quad \varepsilon' = 0.$$

The *reduced* problem, which is found by taking $\varepsilon \rightarrow 0$ in (2.11), reads

$$(2.12a) \quad 0 = u^4 w,$$

$$(2.12b) \quad \dot{w} = u^2,$$

$$(2.12c) \quad 0 = \delta u^4,$$

$$(2.12d) \quad \varepsilon' = 0.$$

For $\delta = 0$, the manifolds \mathcal{S}^0 and \mathcal{M}^0 , as defined in (2.4) and (2.5), respectively, now represent two branches of the *critical manifold* for Equation (2.8); however, neither branch is normally hyperbolic, as the Jacobian of the linearization of the layer flow about both \mathcal{S}^0 and \mathcal{M}^0 is nilpotent. Moreover, as is obvious from (2.12), the reduced flow on \mathcal{S}^0 vanishes, and is hence highly degenerate. Therefore, standard geometric theory does not apply directly.

The underlying non-hyperbolicity can be remedied by means of the blow-up method [3, 4, 12, 13]. A blow-up with respect to ε will allow us to describe the dynamics of (2.2) in a neighborhood of the manifold \mathcal{S}^0 ; cf. Section 3. Our analysis relies on a number of dynamical systems techniques, such as classical geometric singular perturbation theory [5], normal form transformations [30], and the Exchange Lemma [10, 11, 14], the combination of which will result in precise and rigorous asymptotics for Equation (2.8).

To determine the appropriate blow-up transformation, we focus on the (u, w) -subsystem (2.8a)–(2.8b), which for $\varepsilon > 0$ admits two saddle equilibria at $(\pm\varepsilon, 0)$. As we restrict to $u \geq 0$, we consider the positive equilibrium only. The scaling $u = \varepsilon \tilde{u}$ transforms (2.8a)–(2.8b) into

$$\begin{aligned} \tilde{u}' &= \varepsilon^3 \tilde{u}^4 w, \\ w' &= \varepsilon^3 (\tilde{u}^2 - 1), \end{aligned}$$

which yields the integrable system

$$(2.13a) \quad \tilde{u}' = \tilde{u}^4 w,$$

$$(2.13b) \quad w' = \tilde{u}^2 - 1$$

after division through the common factor ε^3 . The saddle equilibrium at $(1, 0)$, together with its stable and unstable manifolds, will play a crucial role in the following; the line $\tilde{u} = 0$ is invariant, with w decreasing thereon. The corresponding phase portrait is shown in [Figure 6](#).

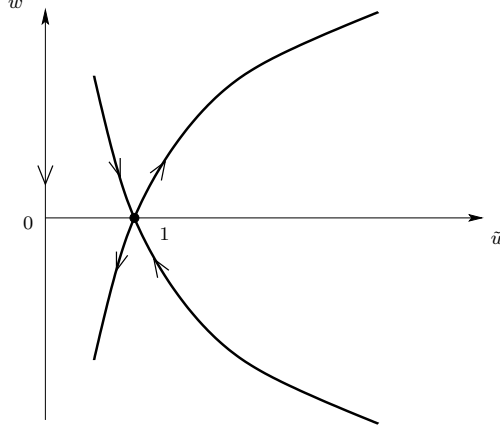


FIGURE 6. The saddle point $(1, 0)$ of System (2.13) and its stable and unstable manifolds.

3. Geometric Desingularization (“Blow-Up”). In this section, we introduce the blow-up transformation that will allow us to desingularize the flow of [Equation \(2.8\)](#) near the non-hyperbolic manifold \mathcal{S}^0 . The discussion at the end of [Section 2](#) suggests the following blow-up:

$$(3.1) \quad u = \bar{r}\bar{u}, \quad w = \bar{w}, \quad \xi = \bar{\xi}, \quad \text{and} \quad \varepsilon = \bar{r}\bar{\varepsilon},$$

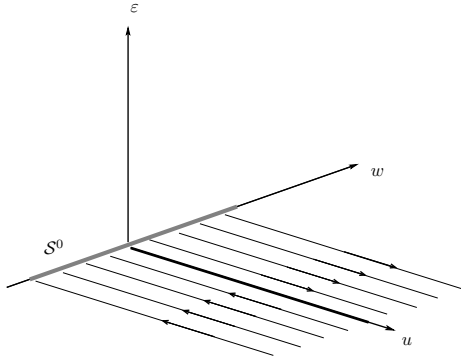
where $(\bar{w}, \bar{\xi}) \in \mathbb{R}^2$ and $(\bar{u}, \bar{\varepsilon}) \in S^1$, *i.e.*, $\bar{u}^2 + \bar{\varepsilon}^2 = 1$. Moreover, $\bar{r} \in [0, r_0)$, with $r_0 > 0$. We note that the equilibrium at $(u, \varepsilon) = (0, 0)$ is blown up to the circle $\{\bar{r} = 0\}$; here, we emphasize that we do not blow up the variables w and ξ .

The vector field that is induced by [\(2.8\)](#) on the cylindrical manifold in $(\bar{u}, \bar{w}, \bar{\xi}, \bar{\varepsilon}, \bar{r})$ -space is best described in coordinate charts. We require two charts here, K_1 and K_2 , which are defined by $\bar{u} = 1$ and $\bar{\varepsilon} = 1$, respectively:

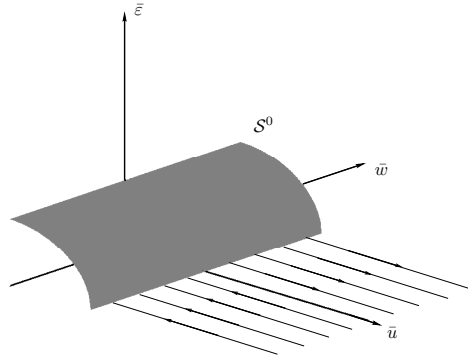
$$(3.2a) \quad K_1 : (u, w, \xi, \varepsilon) = (r_1, w_1, \xi_1, r_1 \varepsilon_1),$$

$$(3.2b) \quad K_2 : (u, w, \xi, \varepsilon) = (r_2 u_2, w_2, \xi_2, r_2).$$

Remark 3.1. The phase-directional chart K_1 describes the “outer” regime, which corresponds to the transient from $u = 1$ to $u = 0$ approaching \mathcal{S}^0 , while the rescaling chart K_2 – also known as the *scaling chart* – covers the “inner” regime where $u \approx 0$, in the context of [Equation \(2.8\)](#); in particular, in chart K_2 , we recover [Equation \(2.13\)](#).



(a) Flow in (u, w, ε) -space; the thick gray line represents the critical manifold S^0 .



(b) Geometry in blown-up $(\bar{u}, \bar{w}, \bar{\varepsilon})$ -space; S^0 is now represented by the cylinder corresponding to $\bar{u}^2 + \bar{\varepsilon}^2 = 1$.

FIGURE 7. Flow of Equation (2.8) for $\varepsilon = 0$ (a) before and (b) after the blow-up in (3.1).

The change of coordinates between charts K_1 and K_2 , which we denote by κ_{12} , can be written as

$$(3.3) \quad \kappa_{12} : (u_2, w_2, \xi_2, r_2) = (\varepsilon_1^{-1}, w_1, \xi_1, r_1 \varepsilon_1),$$

while its inverse κ_{21} is given by

$$(3.4) \quad \kappa_{21} : (r_1, w_1, \xi_1, \varepsilon_1) = (r_2 u_2, w_2, \xi_2, u_2^{-1}).$$

Finally, we define various sections for the blown-up vector field, which will be used

throughout the following analysis: in K_1 , we will require the entry and exit sections

$$(3.5a) \quad \Sigma_1^{\text{in}} := \{(\rho, w_1, \xi_1, \varepsilon_1) \mid w_1 \in [w_-, w_+], \xi_1 \in [\xi_-, \xi_+], \text{ and } \varepsilon_1 \in [0, \sigma]\},$$

$$(3.5b) \quad \Sigma_1^{\text{out}} := \{(r_1, w_1, \xi_1, \sigma) \mid r_1 \in [0, \rho], w_1 \in [w_-, w_+], \text{ and } \xi_1 \in [\xi_-, \xi_+]\},$$

where $0 < \rho < 1$ and $0 < \sigma < 1$ are appropriately defined constants, while w_{\mp} and ξ_{\mp} are real constants, with $w_- < -\frac{2}{\sqrt{3}}$ and $w_+ > \frac{2}{\sqrt{3}}$. Similarly, in chart K_2 , we will employ the section

$$(3.6) \quad \Sigma_2^{\text{in}} := \{(\sigma^{-1}, w_2, \xi_2, r_2) \mid w_2 \in [w_-, w_+], \xi_2 \in [\xi_-, \xi_+], \text{ and } r_2 \in [0, \rho\sigma]\};$$

here, we note that $\Sigma_2^{\text{in}} = \kappa_{21}(\Sigma_1^{\text{out}})$.

Remark 3.2. In the following, we will index a general variable z in blown-up space with \bar{z} . In charts K_i , $i = 1, 2$ that variable will instead be labeled with the corresponding subscript, as z_i .

3.1. Dynamics in chart K_1 . To obtain the equations in K_1 , we substitute the transformation from (3.2a) into Equation (2.8); a straightforward calculation yields

$$(3.7a) \quad r_1' = r_1^4 w_1,$$

$$(3.7b) \quad w_1' = r_1^3 \varepsilon_1 (1 - \varepsilon_1^2),$$

$$(3.7c) \quad \xi_1' = \delta r_1^4,$$

$$(3.7d) \quad \varepsilon_1' = -r_1^3 \varepsilon_1 w_1.$$

Since $\varepsilon = r_1 \varepsilon_1$, the singular limit of $\varepsilon = 0$ corresponds to the restriction of the flow of (3.7) to one of the invariant planes $\{r_1 = 0\}$ or $\{\varepsilon_1 = 0\}$. In order to obtain a non-vanishing vector field for $r_1 = 0$, we desingularize Equation (3.7) by dividing out a factor of r_1^3 from the right-hand sides, which again represents a rescaling of the corresponding independent variable:

$$(3.8a) \quad r_1' = r_1 w_1,$$

$$(3.8b) \quad w_1' = \varepsilon_1 (1 - \varepsilon_1^2),$$

$$(3.8c) \quad \xi_1' = \delta r_1,$$

$$(3.8d) \quad \varepsilon_1' = -\varepsilon_1 w_1.$$

3.2. Dynamics in chart K_2 . The equations in K_2 are obtained by substituting the transformation in (3.2b) into (2.8), which gives

$$(3.9a) \quad u_2' = r_2^3 u_2^4 w_2,$$

$$(3.9b) \quad w_2' = r_2^3 (u_2^2 - 1),$$

$$(3.9c) \quad \xi_2' = \delta r_2^4 u_2^4,$$

$$(3.9d) \quad r_2' = 0.$$

Desingularizing as before, by dividing out a factor of r_2^3 from the right-hand sides in (3.9), we find

$$(3.10a) \quad u_2' = u_2^4 w_2,$$

$$(3.10b) \quad w_2' = u_2^2 - 1,$$

$$(3.10c) \quad \xi_2' = \delta r_2 u_2^4,$$

$$(3.10d) \quad r_2' = 0.$$

Here, we remark that, by construction, Equations (3.10a) and (3.10b) correspond to Equation (2.13).

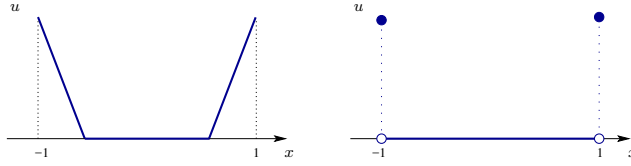
4. Analysis of Bifurcation Diagram – Proof of Theorem 1.3.. In this section, we establish the bifurcation diagram in Figure 3(a) for ε positive and sufficiently small, proving Theorem 1.3. To that end, we investigate the existence and uniqueness of solutions to Equation (2.8), subject to the boundary conditions in (2.9).

All such solutions arise as perturbations of certain limiting solutions that are obtained in the limit of $\varepsilon = 0$. We denote these limiting solutions as singular solutions, as is usual in geometric singular perturbation theory. The approach adopted thereby is the following: first, singular solutions are constructed by analyzing the dynamics in charts K_1 and K_2 separately in the limit as $\varepsilon \rightarrow 0$. Then, the persistence of singular solutions for non-zero ε is shown via the shooting argument outlined in Section 2, which relies on the transversality of the geometric objects involved. That transversality translates into the existence of solutions to the boundary value problem (2.8)–(2.9) along the branches depicted in the bifurcation diagram in Figure 3(a).

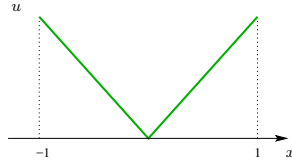
DEFINITION 4.1. *We distinguish three types of singular solutions to the boundary value problem (2.8)–(2.9); see Figure 8:*

- Type I.** *Solutions of type I satisfy $u = 0$ for $x \in I$, where I is an interval centered at $x = 0$. Consequently, the slope of such solutions must initially satisfy $|w| > 1$, in terms of the original w -variable. Type I-solutions, which will henceforth be illustrated in blue, occur in two subtypes: the ones corresponding to $\lambda = \mathcal{O}(\varepsilon)$ have constant finite slope w outside of I , while the ones corresponding to $\lambda = \mathcal{O}(1)$ vanish on $I = (-1, 1)$.*
- Type II.** *Solutions of type II are those of slope $w \equiv \mp 1$, in terms of the original w -variable. These solutions exhibit “touchdown”, reaching $\{u = 0\}$ at one point only, namely at $\xi = 0$. Type II-solutions will be indicated in green in all subsequent figures.*
- Type III.** *Solutions of type III never reach $\{u = 0\}$; hence, no touchdown phenomena occur. These solutions correspond to solutions of the non-regularized model, with $\varepsilon = 0$ in Equation (1.3) [23, 24].*

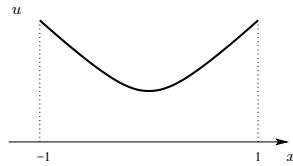
Remark 4.2. The usage of the plural in the definition of type II-solutions requires additional clarification. For Equation (2.2), there exists just one singular solution of type II for $\lambda = 0$ with slope $w = \mp 1$; see the solution labelled d in Figure Figure 2. However, in our blow-up analysis, that singular solution corresponds to a one-parameter family of type II-solutions.



(a) Illustration of type I-solutions for $\lambda = \mathcal{O}(\varepsilon)$ (left panel) and $\lambda = \mathcal{O}(1)$ (right panel).



(b) Type II-solutions.



(c) Type III-solutions.

FIGURE 8. Singular solutions to Equation (2.8), as specified in Definition 4.1.

For $\varepsilon > 0$, we divide the bifurcation diagram in Figure 3(a) into three overlapping regions, as shown in Figure 9.

Remark 4.3. Henceforth, we will refer to the norm $\|u\|_2^2$ in terms of the original variable u in order to be able to compare our analysis with that in [19]; see Figures 2 and 3.

Region \mathcal{R}_1 is defined as

$$(4.1) \quad \mathcal{R}_1 := [0, 1] \times \left[\frac{2}{3} + \nu_1, 2 \right], \quad \text{with } \nu_1 > 0;$$

that region covers the upper part of the bifurcation diagram, where we find the newly emergent branch of solutions for $\varepsilon > 0$ in (1.3) by perturbing from singular solutions of type I. Region \mathcal{R}_2 , which is defined as

$$(4.2) \quad \mathcal{R}_2 := [0, \varepsilon\lambda_2] \times \left[\frac{2}{3} - \nu_2, \frac{2}{3} + \nu_2 \right], \quad \text{with } \lambda_2 > 0 \text{ and } \nu_2 > 0$$

for $\nu_2 > \nu_1$ and λ_2 large, but fixed, represents a small neighborhood of the point B that is depicted as a rectangle in Figure 9. That region shrinks with decreasing ε , collapsing to the segment $\{0\} \times \left[\frac{2}{3} - \nu_2, \frac{2}{3} + \nu_2 \right]$ as $\varepsilon \rightarrow 0$. The branch of solutions contained in this “transition” region is constructed by perturbation from singular

solutions of types I and II. Finally, region \mathcal{R}_3 is defined as

$$(4.3) \quad \mathcal{R}_3 := [0, 1] \times \left[0, \frac{2}{3} + \nu_2\right] \setminus [0, \varepsilon\lambda_3] \times \left[\frac{2}{3} - \nu_3, \frac{2}{3} + \nu_2\right], \quad \text{with } \lambda_3 > 0 \text{ and } \nu_3 > 0,$$

where $\nu_3 < \nu_2$ and λ_3 is again large, but fixed, with $\lambda_3 < \lambda_2$. Region \mathcal{R}_3 covers the lower part of the bifurcation diagram in [Figure 3\(a\)](#), and contains the branch of solutions which is obtained by perturbing from solutions of types II and III.

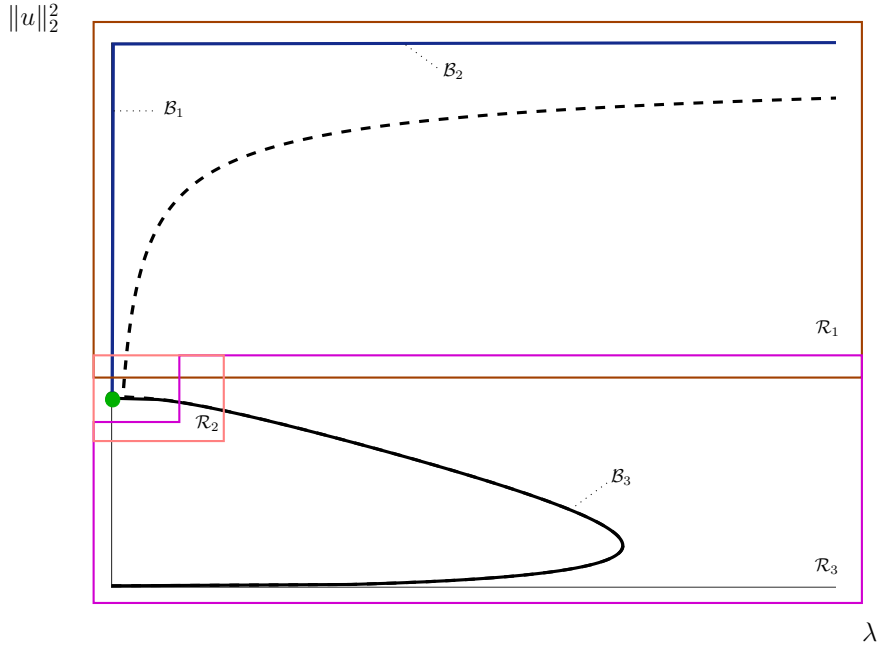


FIGURE 9. Covering of the bifurcation diagram for the boundary value problem (2.8)–(2.9) by three overlapping regions \mathcal{R}_1 (brown), \mathcal{R}_2 (pink), and \mathcal{R}_3 (magenta), for ε positive and small. (For improved visibility, the regions have been extended slightly below $\|u\|_2^2 = 0$, above $\|u\|_2^2 = 2$, and to negative λ , respectively; also, we recall [Remark 4.3](#) with regard to the interpretation of $\|u\|_2^2$ in this context.) The branches of solutions to the boundary value problem (2.8)–(2.9) for $\varepsilon = 0.01$ (dotted curve) and $\varepsilon = 0$ (solid curve) are also displayed. In \mathcal{R}_3 , these branches overlap almost entirely. For $\varepsilon = 0$, the blue branch reduces to the union of a vertical part \mathcal{B}_1 , corresponding to $\lambda = \mathcal{O}(\varepsilon)$, and a horizontal part \mathcal{B}_2 which corresponds to $\lambda = \mathcal{O}(1)$. The green dot at \mathcal{B} represents the singular solution of type II for $\lambda = 0$ that is labeled d in [Figure 2\(a\)](#). The black curve, corresponding to the branch of solutions to the non-regularized model, is labeled \mathcal{B}_3 . In the limit as $\varepsilon \rightarrow 0$, \mathcal{R}_2 shrinks to a segment on the $\|u\|_2^2$ -axis that contains the point \mathcal{B} , cf. (4.2), while region \mathcal{R}_3 grows to a rectangle minus a smaller segment on the $\|u\|_2^2$ -axis containing the point \mathcal{B} ; cf. (4.3).

The true meaning of these regions becomes clearer when we consider a blow-up of the bifurcation diagram in parameter space, *i.e.*, with respect to λ and ε , as illustrated in [Figure 10](#). (That same point of view will also prove useful in parts of the following proofs.) We first embed the diagram, which depends on $(\lambda, \|u\|_2^2)$, into \mathbb{R}^3 by including the third variable ε . Then, we blow up the line $\{(0, 0)\} \times \mathbb{R}$ by introducing \bar{r} , $\bar{\lambda}$, and $\bar{\varepsilon}$ such that

$$\lambda = \bar{r}\bar{\lambda} \quad \text{and} \quad \varepsilon = \bar{r}\bar{\varepsilon}$$

with $\bar{\lambda}^2 + \bar{\varepsilon}^2 = 1$, *i.e.*, for $(\bar{\lambda}, \bar{\varepsilon}) \in S^1$, and $\bar{r} \in [0, r_0)$, where $r_0 > 0$. In the blown-up space $S^1 \times \mathbb{R}^2$, the line $\{(0, 0)\} \times \mathbb{R}$ is hence blown up to a cylinder $S^1 \times \{0\} \times \mathbb{R}$.

After blow-up, the curve of singular solutions obtained for $\varepsilon = 0$ consists of three portions which correspond to singular solutions of types I, II, and III, cf. [Figure 8](#), and which are shown in blue, green, and black, respectively. The black curve (type III) is located in $\bar{\varepsilon} = 0$, while the green curve (type II) lies on the cylinder, *i.e.*, in $\{r = 0\}$, with $\|u\|_2^2 = \frac{2}{3}$ constant. Finally, the blue curve (type I) consists of a branch on the cylinder, corresponding to $\lambda = \mathcal{O}(\varepsilon)$, and of another branch in the plane $\{\bar{\varepsilon} = 0\}$ that corresponds to $\lambda = \mathcal{O}(1)$. In the former case, type I-solutions resemble the one shown in the left panel of [Figure 8\(a\)](#); in the second case, type I-solutions are as in the right panel of [Figure 8\(a\)](#). These two branches correspond to \mathcal{B}_1 and \mathcal{B}_2 , respectively, as defined in [Figure 9](#).

Loosely speaking, in blown-up space, a neighborhood of the green curve is hence covered by region \mathcal{R}_2 and part of \mathcal{R}_3 . The blue curve is mostly covered by region \mathcal{R}_1 , with a small portion close to $\delta = \frac{2}{\sqrt{3}}$ covered by \mathcal{R}_2 . Finally, region \mathcal{R}_3 covers the remainder of the green curve close to $\delta = 0$, and the black curve. The curve obtained for $0 < \varepsilon \ll 1$, which is depicted in red in [Figure 10](#), lifts off from the singular curve corresponding to the limit of $\varepsilon = 0$.

Remark 4.4. When referring to regions \mathcal{R}_i , $i = 1, 2, 3$, in blown-up space, we need to consider the preimages of $\mathcal{R}_i \times [0, \varepsilon_0]$ under the blow-up transformation defined above, strictly speaking. However, for the sake of simplicity, we will use the two notations interchangeably.

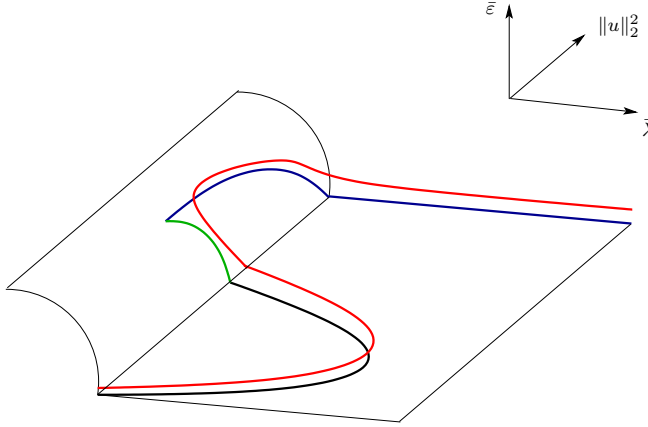


FIGURE 10. Bifurcation diagram for the boundary value problem (2.8)–(2.9) in blown-up parameter space. The singular limit of $\varepsilon = 0$ is represented by the union of the blue, green, and black solid curves, which are covered by \mathcal{R}_1 , \mathcal{R}_2 , and \mathcal{R}_3 , respectively. The portion of the blue curve which lies on the cylinder corresponds to the line \mathcal{B}_1 , while the portion contained in the $\{\bar{\varepsilon} = 0\}$ -plane corresponds to \mathcal{B}_2 . The red curve which lifts off from the $\{\varepsilon = 0\}$ -curve represents solutions to the boundary value problem (2.8)–(2.9) for ε positive, but small.

As stated in [Theorem 1.3](#), we consider $\lambda \in [0, \Lambda]$, where we take $\Lambda = 1$ for the sake of simplicity. In region \mathcal{R}_3 , away from the point B , the perturbation with ε is regular. As will be shown below, singular solutions in regions \mathcal{R}_1 and \mathcal{R}_2 exist only for $\lambda \geq \frac{3}{4}\varepsilon$ or, equivalently, for $\delta \leq \frac{2}{\sqrt{3}}$; cf. [Sections 4.1](#) and [4.2](#). Hence, in these

regions, we need to take $\lambda \in [\frac{3}{4}\varepsilon, 1]$, *i.e.*,

$$(4.4) \quad \delta \in \left[\sqrt{\varepsilon}, \frac{2}{\sqrt{3}} \right],$$

which corresponds to the region shaded in gray in Figure 11.

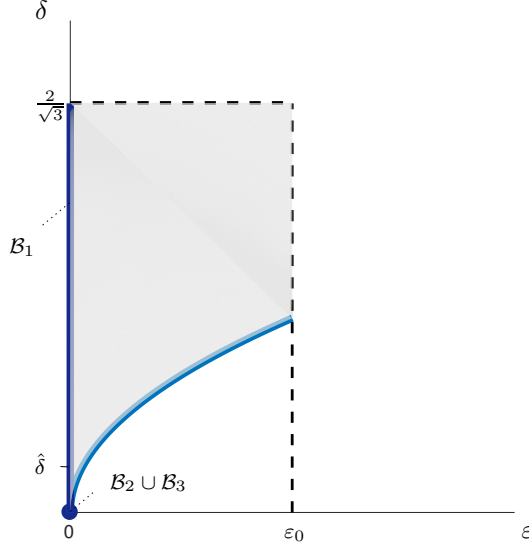


FIGURE 11. Region in (ε, δ) -space, as considered in our analysis. The region, which is shaded in gray, is bounded from below by $\{\delta = \sqrt{\varepsilon}\}$ (light blue curve) and from above by $\{\delta = \frac{2}{\sqrt{3}}\}$ (dashed horizontal line); cf. (4.4). The dark blue segment of the δ -axis corresponds to the union of the two portions of the blue curve shown in Figures 9 and 10. The vertical line corresponds to the line \mathcal{B}_1 , which is divided into two segments at some $\hat{\delta} > 0$ small, while the dot corresponds to the curve $\mathcal{B}_2 \cup \mathcal{B}_3$.

As evidenced in Figure 11, $\delta = 0$ occurs only when $\varepsilon = 0$, which is the point represented by the blue dot therein. The corresponding, highly degenerate limit gives a singular orbit of type I with very singular structure, as shown in the right panel in Figure 8(a). Hence, the whole line \mathcal{B}_2 in the bifurcation diagram for $\varepsilon = 0$ shown in Figure 9 corresponds to that one singular solution.

4.1. Region \mathcal{R}_1 . Region \mathcal{R}_1 in the bifurcation diagram in Figure 9 corresponds to solutions that reduce to those of type I in the singular limit; cf. Definition 4.1. For ε positive and sufficiently small, solutions on that branch come very close to $\{u = \varepsilon\}$; moreover, the length of the interval I where $u \approx \varepsilon$ grows with λ . In the singular limit of $\varepsilon = 0$, the slope of the respective solutions is moderate for $\lambda = \mathcal{O}(\varepsilon)$, corresponding to $0 < \delta < \frac{2}{\sqrt{3}}$, while it tends to infinity for $\lambda = \mathcal{O}(1)$ – *i.e.*, as $\delta \rightarrow 0$ – along the two segments where u changes from $u = 0$ to $u = 1$. These observations are confirmed by the rescaling of w in (2.6): for $\lambda = \mathcal{O}(\varepsilon)$, that rescaling translates into $w = \mathcal{O}(1)$, while it gives $w \rightarrow \infty$ for $\lambda = \mathcal{O}(1)$; cf. Figure 8(a). Interestingly, the proof of our main result in this section, which is stated below, is very similar for these two λ -regimes:

PROPOSITION 4.5. *Given δ_1 fixed, with $0 < \delta_1 < \frac{2}{\sqrt{3}}$ and $\delta_1 \approx \frac{2}{\sqrt{3}}$, there exists $\varepsilon_0 > 0$ sufficiently small such that in region \mathcal{R}_1 , the boundary value problem (2.8)–(2.9) has a unique branch of solutions for $\varepsilon \in (0, \varepsilon_0)$ and $\lambda \in [\frac{\varepsilon}{\delta_1^2}, 1]$. As $\varepsilon \rightarrow 0$, these solutions limit on a singular solution Γ of type I.*

Remark 4.6. The singular solution Γ depends on λ or, equivalently, on δ . Interpreted in terms of δ , the range for which singular solutions exist corresponds to $\delta \in [\sqrt{\varepsilon}, \delta_1]$; recall (2.7).

To prove [Proposition 4.5](#), we construct solutions corresponding to the branch that is contained in region \mathcal{R}_1 for fixed λ in the regime considered here. For δ fixed, a unique singular orbit Γ is determined in blown-up phase space by investigating the dynamics of the boundary value problem (2.8)–(2.9) separately in charts K_1 and K_2 , and by then combining the results obtained in these charts. Finally, the singular orbit Γ , which is essentially determined by the dynamics in chart K_2 , is shown to persist for $0 < \varepsilon \ll 1$.

4.1.1. Dynamics in chart K_2 . The flow of [Equation \(2.8\)](#) from the section Σ_2^{in} back to itself, whereby the sign of w changes from negative to positive, is naturally described in chart K_2 ; cf. [Figure 12](#).

Recalling that $r_2 = \varepsilon$, we observe that [Equation \(3.10\)](#) constitutes a fast-slow system in the standard form of geometric singular perturbation theory [5, 9, 14], with (u_2, w_2) the fast variables and ξ_2 the slow variable. The fast system is given by (3.10), whence the corresponding slow system is obtained by a rescaling of the independent variable with r_2 :

$$\begin{aligned} (4.5a) \quad & r_2 \dot{u}_2 = u_2^4 w_2, \\ (4.5b) \quad & r_2 \dot{w}_2 = u_2^2 - 1, \\ (4.5c) \quad & \dot{\xi}_2 = \delta u_2^4, \\ (4.5d) \quad & \dot{r}_2 = 0. \end{aligned}$$

The associated layer and reduced problems, which are obtained by setting $r_2 = 0$ in (3.10) and (4.5), respectively, read

$$\begin{aligned} (4.6a) \quad & u_2' = u_2^4 w_2, \\ (4.6b) \quad & w_2' = u_2^2 - 1, \\ (4.6c) \quad & \xi_2' = 0, \\ (4.6d) \quad & r_2' = 0 \end{aligned}$$

and

$$\begin{aligned} (4.7a) \quad & 0 = u_2^4 w_2, \\ (4.7b) \quad & 0 = u_2^2 - 1, \\ (4.7c) \quad & \dot{\xi}_2 = \delta u_2^4, \\ (4.7d) \quad & \dot{r}_2 = 0, \end{aligned}$$

respectively. (We note that the (u_2, w_2) -subsystem (4.6a)–(4.6b) is precisely equal to [Equation \(2.13\)](#).) The critical manifold for [Equation \(4.7\)](#) is given by the line

$$(4.8) \quad \mathcal{S}_2^0 := \{(1, 0, \xi_2, 0) \mid \xi_2 \in [\xi_-, \xi_+]\},$$

where the constants ξ_{\mp} are defined as before.

Remark 4.7. While steady states are also found for $u_2 = -1$ in (3.10), these states are irrelevant, since u_2 and r_2 are both non-negative and since $\{u_2 = 0\}$ is an invariant hyperplane for (3.10) which the flow cannot cross.

Linearization of (4.6) about the critical manifold \mathcal{S}_2^0 shows that any point $Q_2 = (1, 0, \xi_2, 0) \in \mathcal{S}_2^0$ is a saddle, with Jacobian

$$\left[\begin{array}{cc} 4u_2^3 w_2 & u_2^4 \\ 2u_2 & 0 \end{array} \right] \Big|_{(u_2, w_2) = (1, 0)} = \left[\begin{array}{cc} 0 & 1 \\ 2 & 0 \end{array} \right]$$

and eigenvalues $\pm\sqrt{2}$. Hence, the manifold \mathcal{S}_2^0 is normally hyperbolic. The reduced flow thereon is described by $\dot{\xi}_2 = \delta$, which corresponds to a constant drift in the positive u_2 -direction with speed δ .

To describe the integrable layer flow away from \mathcal{S}_2^0 , we introduce u_2 as the independent variable, dividing (4.6b) formally by (4.6a):

$$\frac{dw_2}{du_2} = \frac{u_2^2 - 1}{u_2^4 w_2(u_2)}.$$

Solving the above equation with $w_2(1) = 0$, we find

$$(4.9) \quad w_2^\mp(u_2) = \mp \sqrt{\frac{4}{3} - \frac{2}{u_2} + \frac{2}{3u_2^3}}.$$

In particular, it follows from (4.9) that, for any fixed choice of ξ_2 , the stable and unstable manifolds of Q_2 can be written as graphs over u_2 :

$$(4.10a) \quad \mathcal{W}_2^s(Q_2) = \{(u_2, w_2^-(u_2), \xi_2, 0) \mid u_2 \in [1, \infty)\},$$

$$(4.10b) \quad \mathcal{W}_2^u(Q_2) = \{(u_2, w_2^+(u_2), \xi_2, 0) \mid u_2 \in [1, \infty)\}.$$

We have the following result.

LEMMA 4.8. *Let $r_2 \in (0, r_0)$, with r_0 positive and sufficiently small. Then, the following statements hold for Equation (4.5):*

1. *The normally hyperbolic critical manifold \mathcal{S}_2^0 perturbs to a slow manifold*

$$\mathcal{S}_2^{r_2} = \{(1, 0, \xi_2, r_2) \mid \xi_2 \in [\xi_-, \xi_+]\},$$

where ξ_\mp are appropriately chosen constants. In particular, we emphasize that $(u_2, w_2) = (1, 0) \in \mathcal{S}_2^{r_2}$.

2. *The corresponding stable and unstable foliations $\mathcal{F}_2^s(\mathcal{S}_2^{r_2})$ and $\mathcal{F}_2^u(\mathcal{S}_2^{r_2})$ are identical to $\mathcal{F}_2^s(\mathcal{S}_2^0)$ and $\mathcal{F}_2^u(\mathcal{S}_2^0)$, except for their constant r_2 -component. For $r_2 \in [0, r_0)$ fixed, these foliations may be written as*

$$(4.11a) \quad \mathcal{F}_2^s(\mathcal{S}_2^{r_2}) = \{(u_2, w_2^-(u_2), \xi_2, r_2) \mid u_2 \in [1, \infty), \xi_2 \in [\xi_-, \xi_+]\},$$

$$(4.11b) \quad \mathcal{F}_2^u(\mathcal{S}_2^{r_2}) = \{(u_2, w_2^+(u_2), \xi_2, r_2) \mid u_2 \in [1, \infty), \xi_2 \in [\xi_-, \xi_+]\}.$$

Proof. Both statements follow immediately from standard geometric singular perturbation theory [5], in combination with the preceding analysis; in particular, the fact that the plane $\{(u_2, w_2) = (1, 0)\}$ is invariant for Equation (3.10) irrespective of the choice of r_2 implies that the restrictions of $\mathcal{S}_2^{r_2}$ and \mathcal{S}_2^0 to (u_2, w_2, ξ_2) -space do not depend on r_2 . \square

Remark 4.9. The fast-slow structure of Equation (3.10) is very simple, since the (u_2, w_2) -subsystem (3.10a)–(3.10b) decouples from Equation (3.10c). Even for $\varepsilon > 0$, the fast dynamics is determined by that integrable planar system, and organized by the saddle point at $(1, 0)$ and the stable and unstable manifolds thereof. The slow flow on the slow manifold $\mathcal{S}_2^{r_2}$ is just the drift $\dot{\xi} = \delta$.

In the limit as $u_2 \rightarrow \infty$, $w_2^\mp(u_2)$ converges to $w_2^\mp(\infty) = \mp \frac{2}{\sqrt{3}}$; recall (4.9). Transforming the stable manifold $\mathcal{W}_2^s(Q_2)$ and the unstable manifold $\mathcal{W}_2^u(Q_2)$ to chart K_1 , via the coordinate change κ_{21} defined in (3.4), we see that these manifolds limit on the points $(0, \mp \frac{2}{\sqrt{3}}, \xi_1, 0)$, respectively, for ξ_1 fixed; see Figure 12.

4.1.2. Dynamics in chart K_1 . The portions of the singular orbit Γ corresponding to the flow between two sets of boundary conditions that are located at $\xi = \mp 1$ and the section Σ_1^{out} are studied in chart K_1 . A simple calculation reveals that Equation (3.8) admits a line of steady states at

$$(4.12) \quad \mathcal{S}_1^0 := \{(0, 0, \xi_1, 1) \mid \xi_1 \in [\xi_-, \xi_+]\},$$

as well as the plane of steady states

$$(4.13) \quad \pi_1 := \{(0, w_1, \xi_1, 0) \mid w_1 \in [w_-, w_+] \text{ and } \xi_1 \in [\xi_-, \xi_+]\};$$

here, w_\mp and ξ_\mp are defined as in (3.5). (Another set of equilibria, with $\varepsilon_1 = -1$, is irrelevant to us due to our assumption that r_1 and ε_1 are both non-negative.) The line \mathcal{S}_1^0 corresponds to the saddle equilibrium at $(\tilde{u}, w) = (1, 0)$ of Equation (2.13), and coincides with the critical manifold \mathcal{S}_2^0 introduced in chart K_2 ; cf. Equation (4.8).

In chart K_1 , the singular limit of $\varepsilon = 0$ corresponds to either $r_1 = 0$ or $\varepsilon_1 = 0$ in Equation (3.8), which yields the following two limiting systems in the corresponding invariant hyperplanes:

$$(4.14a) \quad r_1' = 0,$$

$$(4.14b) \quad w_1' = \varepsilon_1(1 - \varepsilon_1^2),$$

$$(4.14c) \quad \xi_1' = 0,$$

$$(4.14d) \quad \varepsilon_1' = -\varepsilon_1 w_1$$

and

$$(4.15a) \quad r_1' = r_1 w_1,$$

$$(4.15b) \quad w_1' = 0,$$

$$(4.15c) \quad \xi_1' = \delta r_1,$$

$$(4.15d) \quad \varepsilon_1' = 0,$$

respectively. Equation (4.14) is equivalent to Equation (4.6) in chart K_2 under the coordinate change κ_{21} defined in (3.4); these equations describe the portion of the singular orbit Γ in chart K_1 that is located between Σ_1^{out} and the hyperplane $\{\varepsilon_1 = 0\}$. Equation (4.15), on the other hand, determines the portion of the singular orbit which connects the hyperplane $\{r_1 = 0\}$ with the boundary conditions imposed at $r_1 = 1$. Hence, we first focus our attention on that limiting system.

The value of w_1 in Equation (4.15) is constant: $w_1 \equiv w_0$, for some constant w_0 . Since w_0 must match with the w_2 -value obtained in the limit $u_2 \rightarrow \infty$ in (4.9) in chart K_2 , see Figure 12, $w_1 \equiv \mp \frac{2}{\sqrt{3}}$ must hold in the hyperplane $\{\varepsilon_1 = 0\}$. The corresponding orbits of (4.15) are then easily found by dividing (4.15c) formally by (4.15a): $\frac{d\xi_1}{dr_1} = \frac{\delta}{w_0}$. For any initial condition $\xi_1(1) = \xi_0$, the solution to that equation reads

$$(4.16) \quad \xi_1(r_1) = \frac{\delta}{w_0}(r_1 - 1) + \xi_0.$$

The boundary conditions in (2.9) imply $\xi_0 = \mp 1$; hence, and since $w_0 = \mp \frac{2}{\sqrt{3}}$, we obtain

$$(4.17) \quad \xi_1^\mp(r_1) = \mp \frac{\sqrt{3}}{2} \delta (r_1 - 1) \mp 1.$$

Any orbit of (4.15) can then be written as

$$(4.18) \quad \left\{ \left(r_1, \mp \frac{2}{\sqrt{3}}, \xi_1^\mp(r_1), 0 \right) \mid r_1 \in [0, 1] \right\}.$$

Orbits of the integrable Equation (4.14) can be found by introducing ε_1 as the independent variable: dividing (4.14b) formally by (4.14d), we obtain $\frac{dw_1}{d\varepsilon_1} = -\frac{1-\varepsilon_1^2}{w_1(\varepsilon_1)}$, which can be solved explicitly with $w_1(0) = \mp \frac{2}{\sqrt{3}}$ to yield

$$(4.19) \quad w_1^\mp(\varepsilon_1) = \mp \sqrt{\frac{4}{3} - 2\varepsilon_1 + \frac{2}{3}\varepsilon_1^3},$$

where the sign in (4.19) equals that of the initial w_1 -value. (We remark that (4.19) corresponds to Equation (4.9), after transformation to K_1 -coordinates.) The corresponding values of ξ_1 are constant, and must equal the respective values of $\xi_1^\mp(r_1)$ in (4.17) at $r_1 = 0$, *i.e.*,

$$(4.20) \quad \xi_1^\mp(0) = \pm \frac{\sqrt{3}}{2} \delta \mp 1.$$

Remark 4.10. For $\delta = \frac{2}{\sqrt{3}}$, it follows that $\xi_1^\mp(0) = 0$, *i.e.*, we obtain a singular orbit of type II; see Figures 8(b) and 15. Hence, we must assume $\delta < \frac{2}{\sqrt{3}}$ in the statement of Proposition 4.5.

Any orbit of (4.14) can thus be represented as

$$(4.21) \quad \left\{ (0, w_1^\mp(\varepsilon_1), \xi_1^\mp(0), \varepsilon_1) \mid \varepsilon_1 \in [0, \sigma] \right\},$$

where σ is as in the definition of the section Σ_1^{out} ; recall (3.5).

Concatenation of the two orbit segments defined in Equations (4.18) and (4.21) with the respective signs will yield the singular orbits Γ_1^- and Γ_1^+ , which are located between the sections $\mathcal{V}_{1_0}^-$ and Σ_1^{out} and Σ_1^{out} and $\mathcal{V}_{1_0}^+$, respectively. Here,

$$(4.22) \quad \mathcal{V}_{1_0}^\mp := \left\{ (1, w, \mp 1, 0) \mid w \in I^\mp \right\},$$

with I^\mp being appropriately defined neighborhoods of the points $w_0^- = -\frac{2}{\sqrt{3}}$ and $w_0^+ = \frac{2}{\sqrt{3}}$, respectively; see Figure 12.

4.1.3. Singular orbit Γ . A singular orbit Γ for Equation (2.8) can now be constructed on the basis of the dynamics in charts K_1 and K_2 by taking into account the corresponding boundary conditions in Equation (2.9).

After transformation to K_1 , the manifolds $\mathcal{W}_2^s(Q_2)$ and $\mathcal{W}_2^u(Q_2)$ meet the portions of the orbits Γ_1^- and Γ_1^+ , respectively, as given by (4.21), in the points

$$(4.23) \quad P_1^\mp = \left(0, \mp \frac{2}{\sqrt{3}}, \pm \frac{\sqrt{3}}{2} \delta \mp 1, 0 \right).$$

These points are contained in the two lines

$$(4.24a) \quad \ell_1^- = \left\{ \left(0, -\frac{2}{\sqrt{3}}, \xi_1, 0 \right) \mid \xi_1 \in [\xi_-, \xi_+] \right\},$$

$$(4.24b) \quad \ell_1^+ = \left\{ \left(0, \frac{2}{\sqrt{3}}, \xi_1, 0 \right) \mid \xi_1 \in [\xi_-, \xi_+] \right\},$$

respectively, in the hyperplane $\{\varepsilon_1 = 0\}$, which are both located in the plane of steady states π_1 ; cf. (4.13). The portion of the singular orbit Γ that lies in chart K_1 can hence finally be written as

$$(4.25a) \quad \Gamma_1^- = \left\{ \left(r_1, -\frac{2}{\sqrt{3}}, -\frac{\sqrt{3}}{2}\delta(r_1 - 1) - 1, 0 \right) \mid r_1 \in (0, 1] \right\} \cup P_1^- \\ \cup \left\{ \left(0, -\sqrt{\frac{4}{3} - 2\varepsilon_1 + \frac{2}{3}\varepsilon_1^3}, \frac{\sqrt{3}}{2}\delta - 1, \varepsilon_1 \right) \mid \varepsilon_1 \in (0, \sigma] \right\},$$

$$(4.25b) \quad \Gamma_1^+ = \left\{ \left(r_1, \frac{2}{\sqrt{3}}, \frac{\sqrt{3}}{2}\delta(r_1 - 1) + 1, 0 \right) \mid r_1 \in (0, 1] \right\} \cup P_1^+ \\ \cup \left\{ \left(0, \sqrt{\frac{4}{3} - 2\varepsilon_1 + \frac{2}{3}\varepsilon_1^3}, -\frac{\sqrt{3}}{2}\delta + 1, \varepsilon_1 \right) \mid \varepsilon_1 \in (0, \sigma] \right\}.$$

It remains to identify the portion of Γ that is located in chart K_2 ; we denote the corresponding singular orbit by Γ_2 . We note that, for $r_2 = 0$, Equation (4.6) implies $\xi_2 \equiv \text{constant}$ on Γ_2 . Given the definition of Γ_1^\mp and the fact that $\xi_2 = \xi_1$, we define the points

$$(4.26) \quad Q_2^\mp = \left(1, 0, \pm \frac{\sqrt{3}}{2}\delta \mp 1, 0 \right) \in \mathcal{S}_2^0;$$

therefore, we may write

$$(4.27) \quad \Gamma_2 = \mathcal{W}_2^s(Q_2^-) \cup Q_2^- \cup \left\{ (1, 0, \xi_2, 0) \mid \xi_2 \in \left(\frac{\sqrt{3}}{2}\delta - 1, -\frac{\sqrt{3}}{2}\delta + 1 \right) \right\} \cup Q_2^+ \cup \mathcal{W}_2^u(Q_2^+),$$

recall Equation (4.10), where u_2 now varies in the range $[1, \sigma^{-1}]$. The orbit Γ_2 is hence defined as the union of three segments, with the first being the stable manifold of Q_2^- , the second corresponding to the slow drift in ξ_2 from Q_2^- to Q_2^+ , as shown in the inset of Figure 12, and the third being the unstable manifold of Q_2^+ .

The sought-after singular orbit Γ , which represents the singular solution to the boundary value problem (2.8)–(2.9), is hence given by the union of Γ_1^- , Γ_2 , and Γ_1^+ in blown-up space:

$$\Gamma := \Gamma_1^- \cup \Gamma_2 \cup \Gamma_1^+.$$

A visualization of the orbit Γ is given in Figure 12.

4.1.4. Persistence of Γ – Proof of Proposition 4.5. The proof of Proposition 4.5 is based on the shooting argument outlined in Section 2, which is implemented by approximating the dynamics of Equation (2.8) for ε small in the two coordinate charts K_1 and K_2 . We begin by defining the two manifolds

$$(4.28) \quad \mathcal{V}_{1_\varepsilon}^\mp := \left\{ (1, w, \mp 1, \varepsilon) \mid w \in I^\mp \right\} \quad \text{for } \varepsilon \in [0, \varepsilon_0),$$

which represent the boundary conditions in (2.9) in chart K_1 , with $r_1 = 1$ for $\xi_1 = \mp 1$; hence, it also follows that $\varepsilon_1 = \frac{\varepsilon}{r_1} = \varepsilon$ there. (We note that, for $\varepsilon = 0$, the manifolds $\mathcal{V}_{1_\varepsilon}^\mp$ in (4.28) reduce to $\mathcal{V}_{1_0}^\mp$, respectively, as defined in (4.22).) The intervals I^\mp

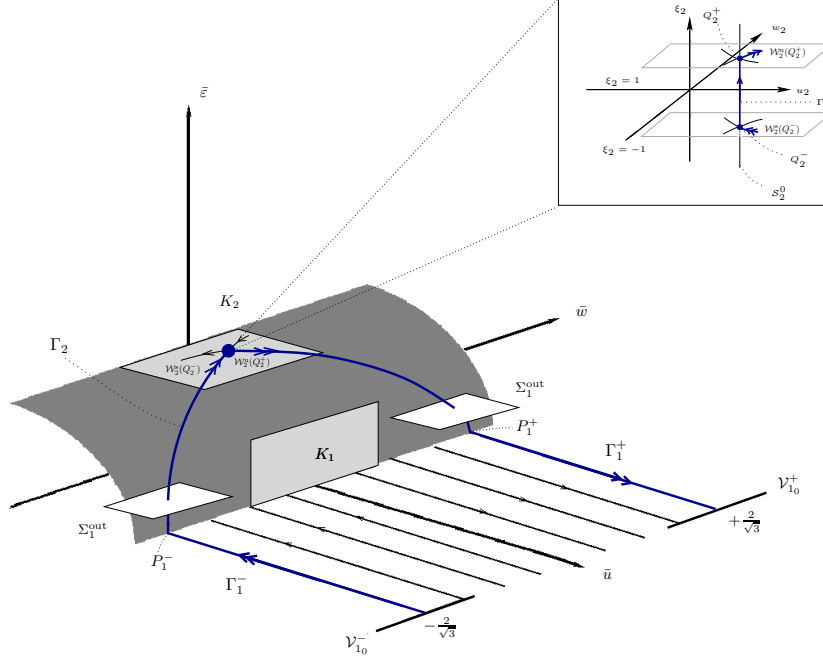


FIGURE 12. Geometry of the singular orbit $\Gamma = \Gamma_1^- \cup \Gamma_2 \cup \Gamma_1^+$ for Equation (2.8) in blown-up space. The orbit Γ is shown in blue, corresponding to a singular solution of type I. The inset resolves in detail the fast-slow structure in (u_2, w_2, ξ_2) -space in chart K_2 ; in particular, the critical manifold S_2^0 and the resulting singular connection between Q_2^- and Q_2^+ is shown.

and I^+ represent appropriately defined neighborhoods of the points $w_0^- = -\frac{2}{\sqrt{3}}$ and $w_0^+ = \frac{2}{\sqrt{3}}$, respectively.

We note that the manifolds $\mathcal{V}_{1_\varepsilon}^\mp$ are mapped onto each other by the transformation $(r_1, w_1, \xi_1, \varepsilon_1) \mapsto (r_1, -w_1, -\xi_1, \varepsilon_1)$, in accordance with the symmetry properties of the boundary value problem (2.8)–(2.9), as discussed in the Introduction. It is hence sufficient to consider the transition from $\mathcal{V}_{1_\varepsilon}^-$ to Σ_1^{out} under the flow of (3.8), as its counterpart, the transition between Σ_1^{out} and $\mathcal{V}_{1_\varepsilon}^+$, can be obtained in a symmetric fashion.

We now introduce ε_1 as the independent variable in Equation (3.8), whence

$$(4.29a) \quad \frac{dr_1}{d\varepsilon_1} = -\frac{r_1}{\varepsilon_1},$$

$$(4.29b) \quad \frac{dw_1}{d\varepsilon_1} = -\frac{1 - \varepsilon_1^2}{w_1(\varepsilon_1)},$$

$$(4.29c) \quad \frac{d\xi_1}{d\varepsilon_1} = -\delta \frac{r_1(\varepsilon_1)}{\varepsilon_1 w_1(\varepsilon_1)}.$$

Here, we remark that $w_1(\varepsilon_1)$ remains non-zero for ε sufficiently small, as we know that $w_1 = \mp \frac{2}{\sqrt{3}} + \mathcal{O}(\varepsilon_1) \neq 0$ in the singular limit, *i.e.*, for $\varepsilon = 0$. Solving Equations (4.29a)

and (4.29b), with initial condition $(1, w, -1, \varepsilon) \in \mathcal{V}_{1\varepsilon}^-$, we find

$$(4.30) \quad r_1(\varepsilon_1) = \frac{\varepsilon}{\varepsilon_1} \quad \text{and} \quad w_1^-(\varepsilon_1) = -\sqrt{w^2 + 2(\varepsilon - \varepsilon_1) - \frac{2}{3}(\varepsilon^3 - \varepsilon_1^3)}.$$

Substituting the expressions in (4.30) into (4.29c) and expanding the result for ε_1 small, we obtain

$$\begin{aligned} \frac{d\xi_1}{d\varepsilon_1} &= \delta \frac{\varepsilon}{\varepsilon_1^2} \frac{1}{\sqrt{w^2 + 2(\varepsilon - \varepsilon_1) - \frac{2}{3}(\varepsilon^3 - \varepsilon_1^3)}} \\ &= \delta \frac{\varepsilon}{\varepsilon_1} \frac{1}{\sqrt{w^2 + 2\varepsilon - \frac{2}{3}\varepsilon^3}} \left[\frac{1}{\varepsilon_1} + \frac{1}{w^2 + 2\varepsilon - \frac{2}{3}\varepsilon^3} \right] + \mathcal{O}(1), \end{aligned}$$

which can be solved to the order considered here and evaluated in Σ_1^{out} – *i.e.*, for $\varepsilon_1 = \sigma$ – to yield

$$(4.31) \quad \xi_1^{\text{out}-} = -1 - \frac{\delta}{w} + \frac{\delta}{w^3} \varepsilon \ln \varepsilon + \mathcal{O}(\varepsilon).$$

Similarly, evaluating (4.30) in Σ_1^{out} , we find

$$\begin{aligned} (r_1^{\text{out-}}, w_1^{\text{out-}}, \xi_1^{\text{out-}}, \varepsilon_1^{\text{out-}}) \\ = \left(\frac{\varepsilon}{\sigma}, -\sqrt{w^2 + 2(\varepsilon - \sigma) - \frac{2}{3}(\varepsilon^3 - \sigma^3)}, -1 - \frac{\delta}{w} + \mathcal{O}(\varepsilon \ln \varepsilon), \sigma \right), \end{aligned}$$

which defines a curve $(w_1^{\text{out-}}, \xi_1^{\text{out-}})(w)$ that is parametrized by the initial w_1 -value w in $\mathcal{V}_{1\varepsilon}^-$. That curve, which we denote by $\mathcal{V}_{1\varepsilon}^{\text{out-}}$, is located in a two-dimensional subset of Σ_1^{out} and, specifically, in the (w_1, ξ_1) -plane, with (r_1, ε_1) fixed:

$$(4.32) \quad \mathcal{V}_{1\varepsilon}^{\text{out-}} := \left\{ \left(-\sqrt{w^2 + 2(\varepsilon - \sigma) - \frac{2}{3}(\varepsilon^3 - \sigma^3)}, -1 - \frac{\delta}{w} + \mathcal{O}(\varepsilon \ln \varepsilon) \right) \mid w \in I^- \right\}.$$

It remains to study the stable foliation $\mathcal{F}_2^s(\mathcal{S}_2^{r_2})$ in coordinate chart K_2 , and to show that the intersection thereof with $\mathcal{V}_{1\varepsilon}^{\text{out-}}$ is transverse for ε sufficiently small. To that end, we recall the definition of $\mathcal{F}_2^s(\mathcal{S}_2^{r_2})$ in (4.11a), which we restrict to the section $\Sigma_2^{\text{in}} = \kappa_{12}(\Sigma_1^{\text{out}})$: taking $r_2 (= \varepsilon)$ fixed, as before, and evaluating $\mathcal{F}_2^s(\mathcal{S}_2^{r_2})$ at $u_2 = \sigma^{-1}$ defines a curve $\mathcal{F}_2^{\text{in-}}$ in Σ_2^{in} which is parametrized by $\xi_2 \in [\xi_-, \xi_+]$ via

$$(u_2^{\text{in}}, w_2^{\text{in}}, \xi_2^{\text{in}}, r_2^{\text{in}}) = \left(\sigma^{-1}, -\sqrt{\frac{4}{3} - 2\sigma + \frac{2}{3}\sigma^3}, \xi_2, r_2 \right),$$

for any $r_2 \in [0, \rho\sigma]$; cf. (3.6). Transforming $\mathcal{F}_2^{\text{in-}}$ to chart K_1 , we obtain the corresponding curve $\mathcal{F}_1^{\text{in-}}$:

$$(4.33) \quad \mathcal{F}_1^{\text{in-}} := (w_1^{\text{out}}, \xi_1^{\text{out}}) = \left\{ \left(-\sqrt{\frac{4}{3} - 2\sigma + \frac{2}{3}\sigma^3}, \xi_1 \right) \mid \xi_1 \in [\xi_-, \xi_+] \right\}.$$

Comparing Equations (4.32) and (4.33) and expanding

$$-\sqrt{w^2 + 2(\varepsilon - \sigma) - \frac{2}{3}(\varepsilon^3 - \sigma^3)} = w + \frac{\varepsilon - \sigma}{w} + \mathcal{O}[(\varepsilon - \sigma)^2]$$

and

$$-\sqrt{\frac{4}{3} - 2\sigma + \frac{2}{3}\sigma^3} = -\frac{2}{\sqrt{3}} + \frac{\sqrt{3}}{2}\sigma + \mathcal{O}(\sigma^2),$$

we conclude that $\mathcal{V}_{1_\varepsilon}^{\text{out}-}$ and $\mathcal{F}_1^{\text{in}-}$ intersect in some point

$$P_1^{\text{out}-} = \left(-\frac{2}{\sqrt{3}} + \mathcal{O}(\varepsilon), -1 - \frac{\delta}{w} + \mathcal{O}(\varepsilon \ln \varepsilon) \right).$$

As the corresponding tangent vectors in the (w_1, ξ_1) -plane are given by $(1, \frac{\delta}{w^2})$ and $(0, 1)$ to leading order, that intersection is transverse for any ε small. More precisely, transversality between $\mathcal{V}_{1_\varepsilon}^{\text{out}-}$ and $\mathcal{F}_1^{\text{in}-}$ occurs already for $\varepsilon = 0$, *i.e.*, in $\{r_1 = 0\}$, which is sufficient for the Exchange Lemma to apply in chart K_2 ; cf. [Figure 13](#). As these two curves perturb smoothly, the transversality of their intersection persists for $\varepsilon \neq 0$, as well.

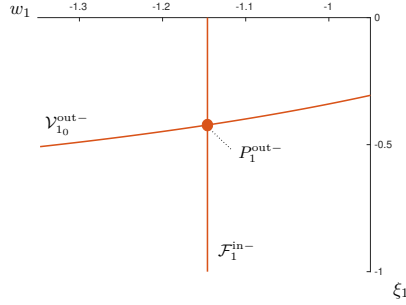


FIGURE 13. *Transversal intersection of the sets $\mathcal{V}_{1_0}^{\text{out}-}$ and $\mathcal{F}_1^{\text{in}-}$ in (w_1, ξ_1) -space.*

Next, and as stated above, the symmetry of [Equation \(3.8\)](#) implies the existence of a point $P_1^{\text{out}+} = (\frac{2}{\sqrt{3}} + \mathcal{O}(\varepsilon), 1 - \frac{\delta}{w} + \mathcal{O}(\varepsilon \ln \varepsilon))$ in Σ_1^{out} in which the curves

$$\mathcal{V}_{1_\varepsilon}^{\text{out}+} = \left\{ \left(\sqrt{w^2 + 2(\varepsilon - \sigma) - \frac{2}{3}(\varepsilon^3 - \sigma^3)}, 1 - \frac{\delta}{w} + \mathcal{O}(\varepsilon \ln \varepsilon) \right) \mid w \in I^+ \right\}$$

and

$$\mathcal{F}_1^{\text{out}+} = \left\{ \left(\sqrt{\frac{4}{3} - 2\sigma + \frac{2}{3}\sigma^3}, \xi_1 \right) \mid \xi_1 \in [\xi_-, \xi_+] \right\}$$

intersect transversely.

In summary, we have hence constructed a connection between the two manifolds of boundary conditions $\mathcal{V}_{1_\varepsilon}^-$ and $\mathcal{V}_{1_\varepsilon}^+$, as follows: in the singular limit of $\varepsilon = 0$, the image $\mathcal{V}_{1_0}^{\text{out}-}$ in Σ_1^{out} of $\mathcal{V}_{1_0}^-$ under the forward flow intersects transversely the equivalent of the stable manifold $\mathcal{W}_2^s(Q_2)$ under the change of coordinates to chart K_1 , namely, $\mathcal{F}_1^{\text{out}-}$. Then, a slow drift occurs along the critical manifold \mathcal{S}_2^0 until the flow leaves along the unstable manifold $\mathcal{W}_2^u(Q_2)$. In Σ_1^{out} , that manifold – which corresponds to $\mathcal{F}_1^{\text{out}+}$ after transformation to K_1 -coordinates – again intersects transversely the image $\mathcal{V}_{1_0}^{\text{out}+}$ of the boundary manifold $\mathcal{V}_{1_0}^+$ under the backward flow. The construction persists for $\varepsilon \neq 0$ sufficiently small; in fact, it guarantees a transversal intersection

between $\mathcal{V}_{1_\varepsilon}^{\text{out}\mp}$ and $\mathcal{F}_1^{\text{out}\mp}$ when $0 < \varepsilon \ll 1$. Finally, the fact that the perturbed orbit approaching the stable foliation of the slow manifold $\mathcal{S}_2^{r_2}$ will leave along the unstable foliation thereof is guaranteed by the Exchange Lemma.

The above argument allows us to obtain the portion of the branch of solutions in the bifurcation diagram which perturbs from \mathcal{B}_1 for $\delta \geq \hat{\delta}$, with $\hat{\delta} > 0$ small; see [Figures 10](#) and [11](#). The portion of the branch perturbing from the part of \mathcal{B}_1 for $0 \leq \delta < \hat{\delta}$, as well as from \mathcal{B}_2 , can be obtained in a similar spirit. However, as that regime involves the limit as $\delta \rightarrow 0$, it requires further consideration. Setting $\delta = 0$ does not affect our construction in chart K_1 ; however, it destroys the slow drift on \mathcal{S}_2^0 in chart K_2 for $\varepsilon = 0$, cf. [Equation \(4.7\)](#).

The segment \mathcal{B}_2 is associated to the regime where $\lambda = \mathcal{O}(1)$. Singular solutions in that regime are of type I; see the right panel of [Figure 8\(a\)](#). We recall that $\delta = 0$ occurs only for $\varepsilon = 0$, cf. [Figure 11](#), and that δ is bounded below by $\sqrt{\varepsilon}$. Hence, it is convenient to introduce the rescaling

$$(4.34) \quad \delta = \sqrt{\varepsilon} \tilde{\delta},$$

with $\tilde{\delta} \geq 1$, which we substitute into the governing [Equations \(3.8\)](#) and [\(3.10\)](#) in charts K_1 and K_2 , respectively. In chart K_1 , the rescaling in [\(4.34\)](#) yields the same dynamics as is obtained by setting $\delta = 0$ in [\(3.8\)](#): the singular limit of $\varepsilon = 0$ implies $\xi_1 \equiv \mp 1$ in the invariant hyperplane $\{\varepsilon_1 = 0\}$; cf. [Equation \(4.15\)](#). It follows that the value of ξ in the transition from $u = 1$ to $u = 0$ does not change, as can also be seen in the corresponding type I-solution; see again the right panel of [Figure 8\(a\)](#). In chart K_2 , introduction of the rescaling in [\(4.34\)](#) again yields a fast-slow system,

$$(4.35a) \quad u'_2 = u_2^4 w_2,$$

$$(4.35b) \quad w'_2 = u_2^2 - 1,$$

$$(4.35c) \quad \xi'_2 = \tilde{\delta} r_2^{\frac{3}{2}} u_2^4,$$

$$(4.35d) \quad r'_2 = 0.$$

The only difference with the previous case of $\delta \neq 0$ is that the slow dynamics is now even slower, as the small perturbation parameter in [\(3.10\)](#) is given by $r_2^{3/2}$, instead of by r_2 . The global construction illustrated in this section is unaffected by that difference, though, as the techniques we have relied on – such as, *e.g.*, the Exchange Lemma – still apply. As $\tilde{\delta}$ grows to $\mathcal{O}(r_2^{-1/2})$, the transition between the two regimes occurs.

Remark 4.11. The presence of an $\varepsilon \ln \varepsilon$ -term in the expansion for ξ_1^{out} in [\(4.31\)](#) is due to resonance between the eigenvalues -1 , 0 (double), and 1 of the linearization of [Equation \(3.8\)](#) about the steady state at $P_1^* = (0, -\frac{2}{\sqrt{3}}, \xi_1^*, 0) \in \pi_1$. The proof is based on a sequence of near-identity normal form transformations in a neighborhood of that state which reduces [\(3.8\)](#) to the system of equations

$$\begin{aligned} r'_1 &= -r_1, \\ \hat{w}'_1 &= \mathcal{O}(3), \\ \hat{\xi}'_1 &= \frac{3\sqrt{3}}{8} \delta \varepsilon + \mathcal{O}(3), \\ \varepsilon'_1 &= \varepsilon_1; \end{aligned}$$

here, $\mathcal{O}(3)$ denotes terms of order 3 and upwards in $(r_1, \hat{w}_1, \hat{\xi}_1, \varepsilon_1)$. One easily sees that the resonant $\frac{3\sqrt{3}}{8}\delta\varepsilon$ -term cannot be removed from the $\hat{\xi}_1$ -equation, resulting in logarithmic switchback after integration; details can be found in [7].

Remark 4.12. We emphasize that the restriction on δ in the statement of [Proposition 4.5](#) is due to the fact that we require $Q_2^- \neq Q_2^+$; cf. also [Remark 4.10](#). Specifically, for the Exchange Lemma to apply, $\frac{\sqrt{3}}{2}\delta - 1 < -\frac{\sqrt{3}}{2}\delta + 1$ must hold, which is equivalent to $\delta < \frac{2}{\sqrt{3}} =: \delta_*$. The case where that condition is violated is studied in [Section 4.2](#) below, which covers region \mathcal{R}_2 . In particular, it is shown there that [Equation \(2.8\)](#) then locally admits a pair of solutions which limit on a solution of type I and one of type II, respectively; these two singular solutions meet in a saddle-node bifurcation at $\delta = \delta_*$.

4.2. Region \mathcal{R}_2 . For $\varepsilon > 0$, region \mathcal{R}_2 covers a small neighborhood of the point B in $(\lambda, \|u\|_2^2)$ -space; recall [Figure 9](#). That region contains the portion of the branch of solutions in the bifurcation diagram which limit on solutions of types I and II as $\varepsilon \rightarrow 0$; moreover, \mathcal{R}_2 establishes the connection with the branches of solutions that are contained in regions \mathcal{R}_1 and \mathcal{R}_3 .

According to the definition in [\(4.2\)](#), the size of \mathcal{R}_2 is ε -dependent; in particular, that region collapses onto a line as $\varepsilon \rightarrow 0$. We will show that, for $0 < \varepsilon \ll 1$, a saddle-node bifurcation occurs in \mathcal{R}_2 at $\lambda = \lambda_*$, as defined in [\[19\]](#); see [Figure 14](#).

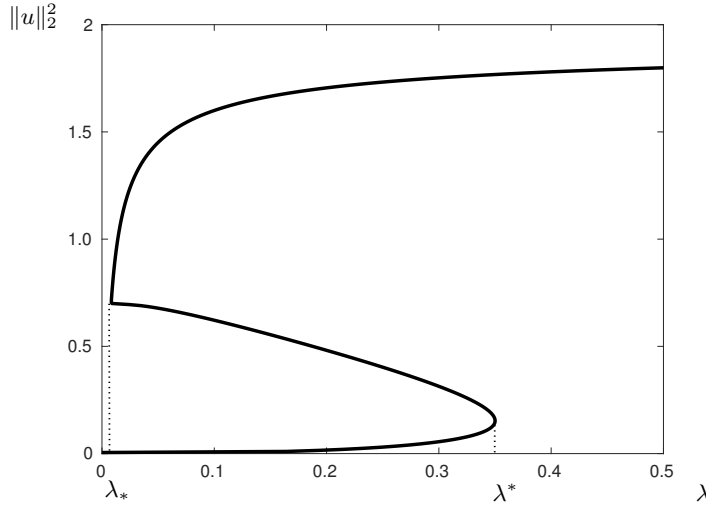


FIGURE 14. Numerical bifurcation diagram showing solutions of [\(1.3\)](#) for $\varepsilon = 0.01$. Saddle-node bifurcations occur at λ_* and λ^* .

Due to the singular dependence of λ_* on the regularization parameter ε , an accurate numerical approximation is difficult to obtain for small values of ε . Using matched asymptotics, it was shown in [\[19\]](#) that $\lambda_* = \mathcal{O}(\varepsilon)$, with an expansion of the form

$$\lambda_*(\varepsilon) = \lambda_{*0}\varepsilon + \lambda_{*1}\varepsilon^2 \ln \varepsilon + \lambda_{*2}\varepsilon^2 + \mathcal{O}(\varepsilon^3).$$

However, the coefficients λ_{*i} remained undetermined there. Here, we confirm rigorously the structure of the above expansion, and we determine explicitly the values of the coefficients λ_{*i} therein for $i = 0, 1$. Moreover, we indicate how higher-order

coefficients may be found systematically, and we identify the source of the logarithmic (“switchback”) terms (in ε) in the expansion for λ_* ; cf. [Proposition 4.16](#) below.

Remark 4.13. While a saddle-node bifurcation is equally observed in the bi-Laplacian case, recall [Equation \(1.2\)](#), Lindsay’s work [20] shows that the asymptotics of the associated λ -value λ_* is far less singular in that case, allowing for a straightforward and explicit calculation of the corresponding coefficients.

To leading order, λ_* equals the abovementioned critical value $\frac{3}{4}\varepsilon$, which corresponds to $\delta_* = \frac{2}{\sqrt{3}}$ in terms of δ . That critical δ -value was not covered in our discussion of region \mathcal{R}_1 in the previous section, as the argument applied in that region failed there; cf. [Remark 4.12](#). Hence, a different argument is required for analysing the local dynamics in a neighborhood of the saddle-node bifurcation point at δ_* .

In a first step, we consider the existence of singular solutions for varying δ ; in particular, the existence of type II-solutions in region \mathcal{R}_2 is guaranteed by the following

LEMMA 4.14. *Let $\frac{1}{\sqrt{\lambda_2}} \leq \delta \leq \delta_1$, with $\delta_1 < \frac{2}{\sqrt{3}}$. Then, a singular solution of type II exists if and only if $w_1 = \mp\delta$ at $\xi_1 = \mp 1$.*

Proof. In the original model, [Equation \(2.1\)](#), the “touchdown” solution of type II satisfies $w = \mp 1$ at $x = \mp 1$; cf. [Definition 4.1](#). After the w -rescaling in [\(2.6\)](#), these boundary conditions are equivalent to $\tilde{w} = \mp\delta$ at $\xi = \mp 1$. The dynamics close to the boundary is naturally studied in chart K_1 , which implies that $w_1 = \mp\delta$ must hold at $\xi_1 = \mp 1$; cf. [\(3.2a\)](#). For $\frac{1}{\sqrt{\lambda_2}} \leq \delta \leq \delta_1$, and in contrast to the solutions of type I considered in [Section 4.1](#), the corresponding orbits can be fully studied in chart K_1 , as they stay away from the critical manifold \mathcal{S}_2^0 in K_2 ; recall [Equation \(4.8\)](#). The existence of a connecting orbit on the blow-up cylinder between $w_1 = -\delta$ and $w_1 = \delta$ then follows automatically; see the upper panel of [Figure 15](#). \square

Remark 4.15. For $\delta = 0$, the type II-solution constructed in [Lemma 4.14](#) collapses onto the line $\{w_1 = 0\}$. That case, which requires further consideration, is studied in region \mathcal{R}_3 ; cf. [Section 4.3](#). In fact, and as previously mentioned, both \mathcal{R}_2 and \mathcal{R}_3 are required to cover the green curve in [Figure 10](#).

[Lemma 4.14](#) guarantees the existence of a type II-solution for every $\delta \in [\frac{1}{\sqrt{\lambda_2}}, \delta_1]$, with $\delta_1 < \delta_*$. For the same range of δ , *i.e.*, in the overlap between regions \mathcal{R}_1 and \mathcal{R}_2 , [Proposition 4.5](#) implies the local existence of type I-solutions. Hence, we can conclude that the boundary value problem [\(2.8\)–\(2.9\)](#) admits a pair of singular solutions for $\delta < \delta_*$; one of these is of type I, while the other is of type II. At $\delta = \delta_*$, the two singular solutions coalesce in a type II-solution. Finally, for $\delta > \delta_*$, no singular solution exists. The resulting three scenarios are illustrated in [Figure 15](#). In particular, we note that solutions of type I satisfy $w_1 = \mp\frac{2}{\sqrt{3}}$ – or, equivalently, $w = \mp\frac{2}{\sqrt{3}\delta}$ in the original formulation – for $\xi_1 = \mp 1$, while those of type II are characterized by $w_1 = \mp\delta$ at $\xi_1 = \mp 1$, as proven in [Lemma 4.14](#); see again [Figure 15](#).

The main result of this section is the following

PROPOSITION 4.16. *There exists $\varepsilon_0 > 0$ sufficiently small such that in region \mathcal{R}_2 , the boundary value problem [\(2.8\)–\(2.9\)](#) admits a unique branch of solutions for $\varepsilon \in (0, \varepsilon_0)$. That branch consists of two sub-branches which limit on singular solutions of types I and II, respectively, as $\varepsilon \rightarrow 0$.*

The two sub-branches meet in a saddle-node bifurcation point at $\lambda_(\varepsilon)$, where two solutions exist for $\lambda > \lambda_*$ and $|\lambda - \lambda_*|$ small, whereas no solution exists for $\lambda < \lambda_*$.*

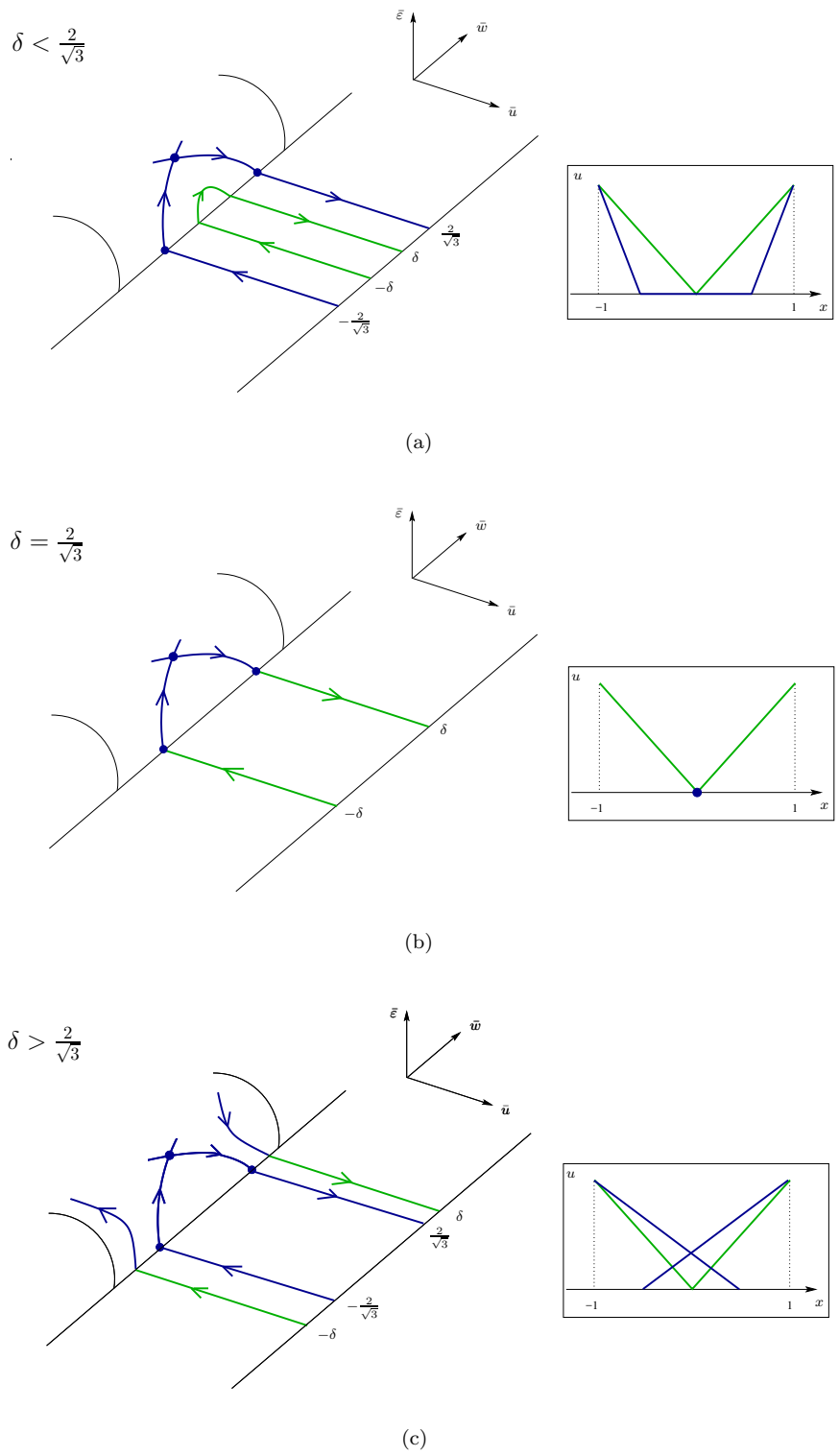


FIGURE 15. Saddle-node bifurcation in the singular limit of $\varepsilon = 0$ in Equation (2.8) upon variation of δ . In the respective insets, the corresponding singular solutions of types I (blue) and II (green) are shown. In particular, for $\delta > \frac{2}{\sqrt{3}}$, no solutions of types I or II exist.

Moreover, for $\varepsilon \in (0, \varepsilon_0)$, λ_* has the asymptotic expansion

$$(4.36) \quad \lambda_*(\varepsilon) = \frac{3}{4}\varepsilon - \left(\sqrt{\frac{3}{2}} + \frac{9}{8}\right)\varepsilon^2 \ln \varepsilon + \mathcal{O}(\varepsilon^2).$$

The transition between regions \mathcal{R}_2 and \mathcal{R}_1 occurs as the branch of solutions limiting on solutions of type I connects to the branch already constructed in [Proposition 4.5](#).

Proof. The proof consists of two parts: we first consider a small neighborhood of $\delta_* = \frac{2}{\sqrt{3}} - i.e.$, of $\lambda = \frac{3}{4}\varepsilon$ – where the saddle-node bifurcation occurs. We define a suitable bifurcation equation, which describes the transition from solutions which limit on type I-solutions to those which limit on solutions of type II. Based on that equation, we infer the presence of the saddle-node bifurcation, and we calculate the expansion of the corresponding λ -value λ_* .

In a second step, we consider the branch of solutions that limit on type II-solutions for the remaining values of λ in \mathcal{R}_2 . Later, that branch will be shown to connect to solutions that are covered by region \mathcal{R}_3 .

We begin by constructing the requisite bifurcation equation for the first step in our proof. Since $w \approx -\frac{2}{\sqrt{3}}$ and $\delta \approx \frac{2}{\sqrt{3}}$, we write

$$(4.37) \quad w_0 = -\frac{2}{\sqrt{3}} + \Delta w \quad \text{and} \quad \delta = \frac{2}{\sqrt{3}} + \Delta \delta.$$

in chart K_1 .

Applying the shooting argument outlined in [Section 2](#), we track the corresponding orbit from the initial manifold $\mathcal{V}_{1_\varepsilon}^-$ defined in [\(4.28\)](#) through K_1 and into the section Σ_1^{out} ; we denote that orbit by γ_1^- . In chart K_2 , the point of intersection of the equivalent orbit γ_2^- with the section Σ_2^{in} is then given by $(\sigma^{-1}, w_2^{\text{in}}, \xi_2^{\text{in}}, \varepsilon)$, for appropriately defined w_2^{in} and ξ_2^{in} .

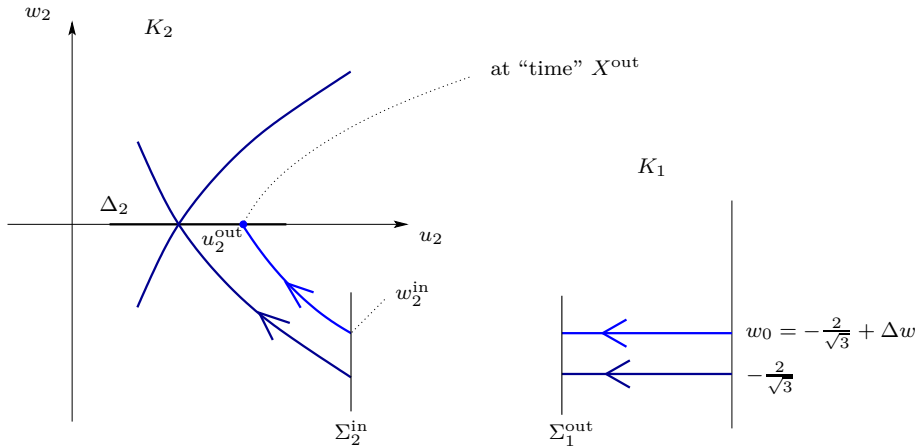


FIGURE 16. Sketch of the shooting argument underlying the proof of [Proposition 4.16](#).

Next, we consider the evolution of the orbit γ_2^- through K_2 . Let X^{out} denote the “time” at which γ_2^- reaches the hyperplane $\Delta_2 = \{w_2 = 0\}$, viz. $w_2(X^{\text{out}}) = 0$. (By symmetry, it then follows that the reflection γ_2^+ of γ_2^- under the map $(u_2, w_2, \xi_2, r_2) \mapsto (u_2, -w_2, -\xi_2, r_2)$ will satisfy the boundary condition at $\mathcal{V}_{1_\varepsilon}^+$, with $w_0 = \frac{2}{\sqrt{3}} - \Delta w$,

after transformation to K_1 .) Clearly, X^{out} depends on w_2^{in} and, in particular, on Δw , *i.e.*, on the initial deviation of the orbit from its singular limit Γ_1^- in chart K_1 .

As per our shooting argument, we need to impose the constraint that $\xi_2(X^{\text{out}}) = 0$. Dividing Equation (3.10c) by Equation (3.10a) and recalling that $r_2 = \varepsilon$ in chart K_2 , we find $\frac{d\xi_2}{du_2} = \frac{\delta\varepsilon}{w_2}$ and, therefore,

$$(4.38) \quad \xi_2(u_2) = \xi_2^{\text{in}} + \delta\varepsilon \int_{u_2^{\text{in}}}^{u_2^{\text{out}}} \frac{1}{w_2(u_2)} du_2.$$

Here, $u_2^{\text{in}} = \sigma^{-1}$ as in the definition of Σ_2^{in} in (3.6), while u_2^{out} denotes the value of u_2 such that $w_2(u_2^{\text{out}}) = 0$; cf. again Figure 16.

The sought-after bifurcation equation now corresponds to a relation between Δw , ε , and δ that is satisfied for any solution to the boundary value problem (2.8)–(2.9) close to the saddle-node bifurcation in Equation (2.8). To derive such a relation, we must first approximate u_2^{out} : recalling the explicit expression for $w_1(\varepsilon_1)$ on γ_1^- , as given in (4.30), substituting the Ansatz made in Equation (4.37), and rewriting the result in the coordinates of chart K_2 , we find

$$(4.39) \quad w_2(u_2) = -\sqrt{\left(-\frac{2}{\sqrt{3}} + \Delta w\right)^2 + 2\left(\varepsilon - \frac{1}{u_2}\right) - \frac{2}{3}\left(\varepsilon^3 - \frac{1}{u_2^3}\right)}$$

on γ_2^- . Next, we write $u_2^{\text{out}} = 1 + \Delta u$ in (4.39), where Δu is assumed to be sufficiently small due to the fact that we stay close to the equilibrium at $(u_2, w_2) = (1, 0)$ in K_2 . Then, we solve the resulting expression for Δu to find three roots; two of these are complex conjugates, and are hence irrelevant due to the real nature of our problem. Expanding the third root, which is real independently of the value of Δw , in a series with respect to Δw and ε , we find

$$(4.40) \quad u_2^{\text{out}} = 1 + \frac{13\sqrt{3}}{9}\Delta w - \frac{13}{6}\varepsilon + \mathcal{O}(2),$$

to first order in Δw and ε .

It remains to determine the leading-order asymptotics of the integral in (4.38). To that end, we expand the integrand therein as

$$(4.41) \quad \frac{1}{w_2(u_2)} = -\sqrt{\frac{3u_2^3}{2(u_2 - 1)^2(2u_2 + 1)}} + \mathcal{O}(\Delta w, \varepsilon),$$

which can be shown to be sufficient to the order of accuracy considered here. (The inclusion of higher-order terms in (4.38) would yield a refined bifurcation equation, and would hence allow us to take the expansion for λ_* in (4.36) to higher order in ε .)

Combining (4.41) and (4.40) and noting that u_2^{in} only enters through higher-order terms in Δw , which are neglected here, we finally obtain the expansion

$$(4.42) \quad \int_{u_2^{\text{in}}}^{u_2^{\text{out}}} \frac{1}{w_2(u_2)} du_2 = -\frac{\sqrt{2}}{2} \ln \Delta w + C + \mathcal{O}(\Delta w)$$

where C is a computable constant. (The above expansion reflects the fact that, as $\Delta w \rightarrow 0$, *i.e.*, as the point $(\sigma^{-1}, w_2^{\text{in}}, \xi_2^{\text{in}}, \varepsilon)$ tends to the stable manifold $\mathcal{W}_2^s(Q_2)$, the “time” required for reaching Δ_2 tends to infinity. Moreover, it is consistent with the

observation that expansions of solutions passing close to equilibria or slow manifolds of saddle type frequently involve logarithmic terms.)

Next, we substitute $\xi_2^{\text{in}} (= \xi_1^{\text{out}}) = -1 - \frac{\delta}{w_0} + \frac{\delta}{w_0^3} \varepsilon \ln \varepsilon + \mathcal{O}(\varepsilon)$ from (4.31) into (4.42) to obtain

$$(4.43) \quad \xi_2(u_2^{\text{out}}) = -1 - \frac{\delta}{w_0} - \frac{\sqrt{2}}{2} \delta \varepsilon \ln \Delta w + \frac{\delta}{w_0^3} \varepsilon \ln \varepsilon + \mathcal{O}(\varepsilon) \stackrel{!}{=} 0.$$

Shifting w_0 and δ by Δw and $\Delta \delta$, cf. (4.37), and solving (4.43) for $\Delta \delta$, we obtain the following bifurcation equation in $(\Delta w, \Delta \delta, \varepsilon)$:

$$(4.44) \quad \Delta \delta = -\Delta w + \frac{2\sqrt{2}}{3} \varepsilon \ln \Delta w + \frac{\sqrt{3}}{2} \varepsilon \ln \varepsilon + \mathcal{O}(\varepsilon).$$

The last step consists in finding the Δw -value Δw_* at which the bifurcation equation in (4.44) attains its minimum, corresponding to the approximate location of the saddle-node bifurcation in Equation (2.8), and in reverting to the original scalings. To that aim, we differentiate Equation (4.44) and solve $\frac{d\Delta\delta}{d\Delta w} = 0$ to leading order, which yields $\Delta w_* = \frac{2\sqrt{2}}{3} \varepsilon$; see Figure 17.

Substituting into (4.44), we hence obtain the corresponding value of $\Delta \delta_*$, which implies $\lambda_* = \frac{\varepsilon}{\delta_*^2} = \varepsilon \left(\frac{2}{\sqrt{3}} + \Delta \delta_* \right)^{-2}$ by Equation (4.37). Hence, we obtain the desired asymptotic expansion for λ_* , viz.

$$(4.45) \quad \lambda_*(\varepsilon) = \frac{3}{4} \varepsilon - \left(\sqrt{\frac{3}{2}} + \frac{9}{8} \right) \varepsilon^2 \ln \varepsilon + \mathcal{O}(\varepsilon^2),$$

as claimed. Finally, since

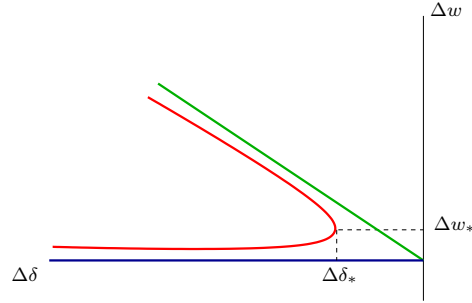
$$\left. \frac{d^2 \Delta \delta}{d(\Delta w)^2} \right|_{\Delta w = \Delta w_*} = -\frac{2\sqrt{2}}{3} \frac{\varepsilon}{(\Delta w_*)^2}$$

is negative, the function $\Delta \delta(\Delta w)$ is locally concave, which implies that the unfolding of solutions to Equation (2.8) for $|\lambda - \lambda_*|$ small is as given in the statement of the proposition; see Figure 17(a). In particular, the branch of solutions which limits on solutions of type I overlaps with the one contained in region \mathcal{R}_1 , as δ_1 can be chosen arbitrarily close to $\frac{2}{\sqrt{3}}$ in the statement of Proposition 4.5.

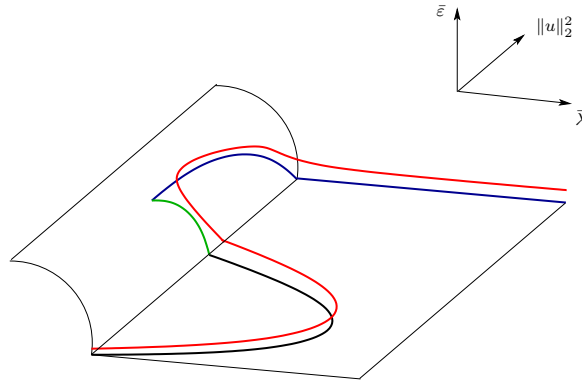
The last part of the proof concerns the existence of solutions to the boundary value problem (2.8)–(2.9) which limit on type II-solutions as $\varepsilon \rightarrow 0$ for the remaining values of λ in \mathcal{R}_2 , i.e., for $\delta \in (\frac{1}{\sqrt{\lambda_2}}, \delta_1)$. The existence of singular solutions of type II in that range is ensured by Lemma 4.14. In the singular limit, i.e., for $\varepsilon = 0$, we have transversality at $\xi_1 = 0$ with respect to variation of w_1 at $\xi_1 = \mp 1$ around $\mp \delta$. Hence, the corresponding singular solutions perturb to solutions of the boundary value problem (2.8)–(2.9) for $0 < \varepsilon \ll 1$, which completes the proof. \square

Remark 4.17. The branch of solutions derived in the last part of the proof is still described by the bifurcation equation in (4.44), the difference being that the $\varepsilon \ln \Delta w$ -term is now regular, i.e., $\mathcal{O}(\varepsilon)$, due to $\Delta w = \mathcal{O}(1)$. The above proof also implies that $\Delta \delta$ must be larger than $\mathcal{O}(\varepsilon)$; in fact, Lindsay's work [19] shows that $\Delta \delta = \mathcal{O}(\varepsilon \ln \varepsilon)$.

Remark 4.18. The presence of an $\varepsilon \ln \varepsilon$ -term in the bifurcation equation (4.44) implies that the convergence to the singular limit of $\varepsilon = 0$ cannot be smooth in ε ; rather, it will be regular in $(\varepsilon, \ln \varepsilon)$. A similar situation was encountered in Proposition 4.5 above, where the presence of logarithmic switchback terms in ε was observed; recall Remark 4.11.



(a) Local view.



(b) Global view.

FIGURE 17. Illustration of the saddle-node bifurcation at λ_* in Equation (2.8). The red curve corresponds to the case of $\varepsilon \neq 0$, while the singular limit of $\varepsilon = 0$ is represented in blue (type I), green (type II), and black (type III). The point of intersection of the green and blue curves corresponds to the critical δ -value δ_* ; a small neighborhood of that point where the transition between these two curves occurs is considered in the first part of Proposition 4.16, while the remainder of the green curve – up to an arbitrarily small, but fixed distance from the intersection with the black curve – is studied in the second part of Proposition 4.16. Finally, the transition between the green and black curves is described in Section 4.3 below.

The asymptotic expansion for λ_* in (4.36) shows excellent agreement with numerical values that were obtained using the continuation software package AUTO [2]; see Figure 18. In particular, the distance between the two curves is $\mathcal{O}(\varepsilon^2)$, *i.e.*, of higher order in ε , as postulated.

4.3. Region \mathcal{R}_3 . It remains to analyse region \mathcal{R}_3 , which contains the branch of solutions in the bifurcation diagram that perturb from type III-solutions, corresponding to the non-regularized problem

$$(4.46) \quad u'' = \frac{\lambda}{u^2}, \quad \text{for } x \in [-1, 1], \text{ with } u = 1 \text{ when } x = \mp 1.$$

By Definition 4.1, solutions of type III differ from those of types I and II, in that they do not exhibit touchdown phenomena. Regularization affects them only weakly, *i.e.*, in a regular fashion, with the effect becoming slightly more pronounced as $\lambda \rightarrow 0$;

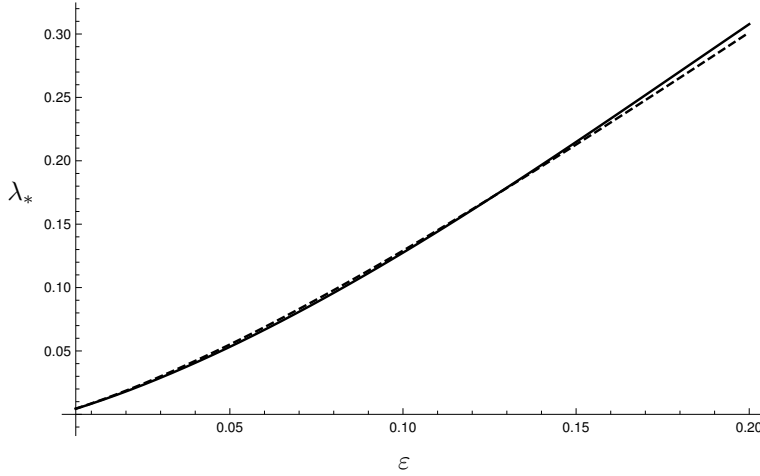


FIGURE 18. Comparison between the asymptotic expansion for $\lambda_*(\varepsilon)$ in (4.36) (solid curve) and numerical values obtained with AUTO (dashed curve).

cf. Figure 19. Thus, most of the solutions contained in region \mathcal{R}_3 perturb from \mathcal{B}_3 in a regular way, and are hence easy to obtain. The limit of $\lambda \rightarrow 0$, i.e., the transition from \mathcal{R}_3 to \mathcal{R}_2 , needs to be treated more carefully.

Remark 4.19. It is easy to see that Equation (4.46) – or, rather, the corresponding first-order system – is Hamiltonian; the level curves of the associated Hamiltonian are given precisely by the singular solutions in panel (b) of Figure 19.

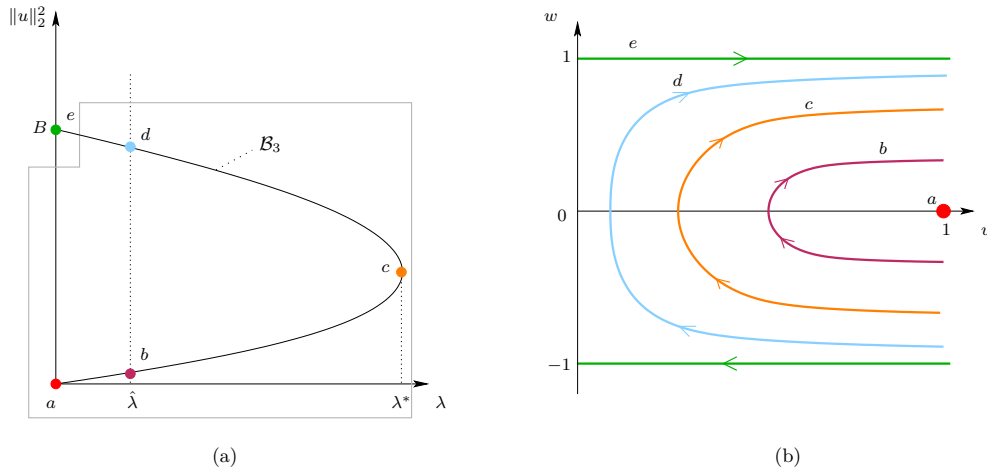


FIGURE 19. (a) Covering of the curve \mathcal{B}_3 by region \mathcal{R}_3 for $\varepsilon > 0$; (b) the corresponding singular solutions in the original (u, w) -space. The green solution is of type II, and corresponds to the limit as $\lambda \rightarrow 0$. Recall that, for $\varepsilon \rightarrow 0$, \mathcal{R}_3 approaches the line $\{\lambda = 0\}$ near the point B . Singular solutions corresponding to $\lambda > 0$ are of type III and do not exhibit touchdown phenomena. The orange solution realized at the fold point $\lambda = \lambda^*$ is the one where the two parts of the curve \mathcal{B}_3 meet.

Type III-solutions are contained in the curve \mathcal{B}_3 in the limit of $\delta = 0$; see Figure 11. That limit was not covered in region \mathcal{R}_2 , as the approach used there required the

assumption that $\delta \geq \frac{1}{\sqrt{\lambda_2}}$. The limit as $\delta \rightarrow 0$, however, results in singular dynamics in chart K_1 , as the type II-solution (green) – corresponding to $w_1 = \mp\delta$ at $\xi_1 = \mp 1$ – collapses onto the line

$$(4.47) \quad \mathcal{M}_1^0 := \{(r_1, 0, \xi_1, 0) \mid r_1 \in \mathbb{R}^+, \xi_1 \in \mathbb{R}\};$$

see Figure 5 and the upper panel of Figure 15. Clearly, \mathcal{M}_1^0 constitutes a line of non-hyperbolic equilibria for Equation (3.8) which corresponds to the manifold \mathcal{M}^0 in (2.5), after blow-down. The singular nature of \mathcal{M}_1^0 is related to the rescaling of w introduced in (2.6). That rescaling, which corresponded to “zooming out”, turned out to be particularly useful for our analysis in regions \mathcal{R}_1 and \mathcal{R}_2 . However, it cannot provide a good description of region \mathcal{R}_3 . To study the dynamics in \mathcal{R}_3 , we would have to perform another blow-up involving δ , w_1 , and ε_1 in chart K_1 in order to basically undo the w -rescaling in (2.6). It is much simpler to consider the δ -range covered by \mathcal{R}_3 by returning to the original system without any rescaling of w ; cf. Equation (2.2).

The main result of this section is the following:

PROPOSITION 4.20. *There exists $\varepsilon_0 > 0$ sufficiently small such that in region \mathcal{R}_3 , the boundary value problem (2.2)–(2.3) admits a unique branch of solutions for $\varepsilon \in (0, \varepsilon_0)$. Outside of a fixed neighborhood of the point B , that branch converges smoothly as $\varepsilon \rightarrow 0$ to the curve \mathcal{B}_3 along which solutions of the non-regularized boundary value problem, Equation (4.46), exist. In the ε -dependent region overlapping with \mathcal{R}_2 , the branch of solutions limiting on solutions of type II described in Proposition 4.16 is recovered. There, the transition from solutions that limit on type-III solutions to those limiting on singular solutions of type II occurs.*

Proof. We recall the original first-order system, Equation (2.2):

$$\begin{aligned} u' &= u^4 w, \\ w' &= \lambda(u^2 - \varepsilon^2), \\ \xi' &= u^4, \\ \varepsilon' &= 0; \end{aligned}$$

given Equation (2.7), we write $\varepsilon = \delta^2 \lambda$ and obtain the equivalent system

$$\begin{aligned} (4.48a) \quad u' &= u^4 w, \\ (4.48b) \quad w' &= \lambda(u^2 - \delta^4 \lambda^2), \\ (4.48c) \quad \xi' &= u^4, \\ (4.48d) \quad \delta' &= 0. \end{aligned}$$

Here, the parameter δ plays the role of the small perturbation parameter, with the δ -range corresponding to region \mathcal{R}_3 given by

$$\delta \in \left[0, \frac{1}{\sqrt{\lambda_3}}\right];$$

cf. (4.3). In summary, it is hence more convenient to consider λ and δ , rather than λ and ε , as the relevant parameters in this regime.

For $\delta = 0$ and $\lambda > 0$, the projection of the flow of Equation (4.48) is as illustrated in Figure 4. In region \mathcal{R}_3 , however, we are also interested in covering a small neighborhood of $\lambda = 0$, which again gives the singular dynamics shown in Figure 5.

In (u, w) -space, the singular solution found for $\lambda = 0$ consists of $[0, 1] \times \{-1\}$ and $[0, 1] \times \{1\}$, *i.e.*, it approaches the degenerate line of equilibria for (4.48) at $\{(0, w)\}$ under the forward and backward flow in x , respectively; see Figure 20.

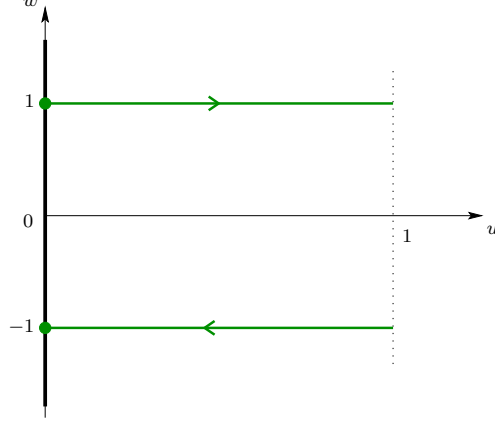


FIGURE 20. Singular solution of Equation (4.48) for $(\delta, \lambda) = (0, 0)$ in (u, w) -space. That solution, which is of type II, cf. Figure 8(b), is shown in green. The solid black line represents the degenerate line of equilibria at $\{(0, w)\}$.

To analyze the dynamics close to that line, we have to introduce a blow-up of $(u, \lambda) = (0, 0)$. As the blow-up involves λ , we append the trivial equation $\lambda' = 0$ to (4.48):

$$(4.49a) \quad u' = u^4 w,$$

$$(4.49b) \quad w' = \lambda(u^2 - \delta^4 \lambda^2),$$

$$(4.49c) \quad \xi' = u^4,$$

$$(4.49d) \quad \lambda' = 0,$$

$$(4.49e) \quad \delta' = 0.$$

The requisite blow-up transformation is then given by

$$(4.50) \quad u = \bar{r}\bar{u} \quad \text{and} \quad \lambda = \bar{r}\bar{\lambda},$$

where $(\bar{u}, \bar{\lambda}) \in S^1$, *i.e.*, $\bar{u}^2 + \bar{\lambda}^2 = 1$, and $\bar{r} \in [0, r_0)$, with $r_0 > 0$. We denote the chart corresponding to $\bar{u} = 1$ by κ_1 . The analysis in that chart turns out to be sufficient for proving Proposition 4.20. In chart κ_1 , the blow-up transformation in (4.50) reads

$$(4.51) \quad u = r_1 \quad \text{and} \quad \lambda = r_1 \lambda_1.$$

which gives

$$(4.52a) \quad r_1' = r_1 w,$$

$$(4.52b) \quad w' = \lambda_1(1 - \delta^4 \lambda_1^2),$$

$$(4.52c) \quad \xi' = r_1,$$

$$(4.52d) \quad \lambda_1' = -\lambda_1 w,$$

$$(4.52e) \quad \delta' = 0$$

for Equation (4.49) in that chart; here, δ is the small (regular) perturbation parameter. For any $\lambda \in [0, 1]$, the existence of solutions to (4.52) can be studied via the symmetric shooting argument outlined in Section 2. To that end, we define a set of initial conditions at $(r_1, \xi) = (1, -1)$, as follows:

$$(4.53) \quad \mathcal{V}_\lambda = \{(1, w_0, -1, \lambda, \delta) \mid w_0 \in I\},$$

where I is a neighborhood of $w = -1$. We remark that the initial value λ for λ_1 follows from $\lambda = r_1 \lambda_1$, cf. (4.51), as $r_1 = 1$ initially. Next, we introduce w as the independent variable in (4.52), whence

$$(4.54a) \quad \frac{dr_1}{dw} = \frac{r_1 w}{\lambda_1 (1 - \delta^4 \lambda_1^2)},$$

$$(4.54b) \quad \frac{d\xi}{dw} = \frac{r_1}{\lambda_1 (1 - \delta^4 \lambda_1^2)},$$

$$(4.54c) \quad \frac{d\lambda_1}{dw} = -\frac{w}{1 - \delta^4 \lambda_1^2},$$

$$(4.54d) \quad \frac{d\delta}{dw} = 0,$$

with initial conditions

$$(4.55) \quad r_1(w_0) = 1, \quad \xi(w_0) = -1, \quad \lambda_1(w_0) = \lambda, \quad \text{and} \quad \delta(w_0) = 0.$$

We track \mathcal{V}_λ under the flow of (4.54) up to the hyperplane $\{w = 0\}$; see Figure 21. There, we obtain a point $(r_1^{\text{out}}, 0, \xi^{\text{out}}, \lambda_1^{\text{out}}, \delta)$ in $(r_1, w, \xi, \lambda_1, \delta)$ -space. Our shooting argument implies that we have to solve the equation

$$(4.56) \quad \xi^{\text{out}}(w_0, \lambda, \delta) = 0.$$

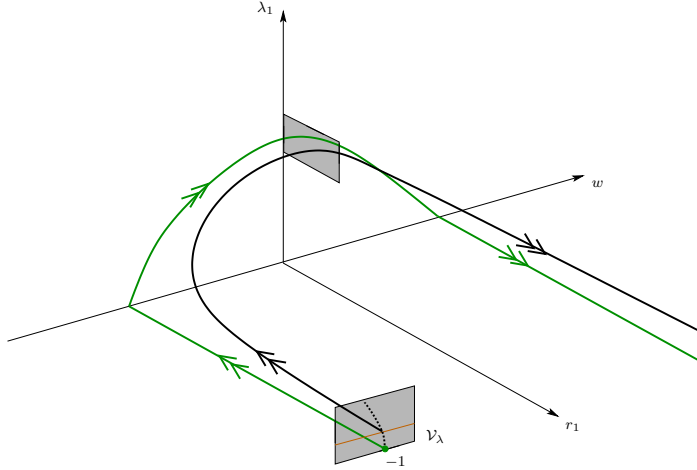


FIGURE 21. Dynamics of Equation (4.52) in (r_1, w, λ_1) -space. The gray section at $r_1 = 0$ corresponds to \mathcal{V}_λ , cf. (4.53), which is flown forward to $\{w = 0\}$. The green orbit represents the singular solution for $\lambda = 0$, i.e., a singular solution of type II, which satisfies $w = -1$ at $\xi = -1$. The black orbit corresponds to a solution of (4.52) with initial conditions in \mathcal{V}_λ for a fixed value of $\lambda > 0$ and $\delta = 0$, which is a solution of type III. The dashed curve contained in \mathcal{V}_λ corresponds to the set $\{w_0 = w_0(\lambda)\}$ that solves Equation (4.58). That set is defined by Equation (4.59) for $\delta = 0$. The orange line indicates a section through \mathcal{V}_λ for fixed $\lambda > 0$.

At this point, we split \mathcal{R}_3 into two subregions in which we apply separate arguments to prove the existence of a unique branch of solutions, as claimed in the statement of the proposition. For $\lambda \geq \tilde{\lambda}$, with $\tilde{\lambda}$ fixed and positive, and $\delta = 0$, Equation (4.54) can be solved explicitly subject to (4.55); moreover, a solution $w_0 = w_0(\lambda)$ of Equation (4.56) can be proven to exist for $\lambda \leq \lambda^*$. At $\lambda = \lambda^*$, transversality breaks down, as Equation (4.56) does not admit a solution for $\lambda > \lambda^*$. The corresponding singular solutions are of type III; cf. Definition 4.1. Due to the regularity of (4.56) with respect to δ , these solutions perturb in a regular fashion to solutions of (4.54)–(4.55) for δ positive and small; in particular, we consider $\delta \leq \frac{1}{\sqrt{\lambda_3}}$ with λ_3 large, in accordance with (4.3). For λ close to λ^* , individual solutions do not perturb regularly; however, the structurally stable saddle-node bifurcation at λ^* as a whole will persist as a regular perturbation, giving rise to a slightly perturbed value $\lambda^*(\delta)$ for the perturbed saddle-node point. Since the resulting asymptotics of $\lambda^*(\delta)$ is not our main concern, we do not consider it further here.

The second subregion of \mathcal{R}_3 , which includes the overlap with region \mathcal{R}_2 , corresponds to a small neighborhood of $(\lambda, \delta) = (0, 0)$ that is given by

$$(4.57) \quad (\lambda, \delta) \in [0, \tilde{\lambda}] \times \left[0, \frac{1}{\sqrt{\lambda_3}}\right].$$

To study the branch of solutions in this subregion, we solve Equation (4.54) with initial conditions as in (4.55) by expanding around $(w_0, \lambda, \delta) = (-1, 0, 0)$, and by making use of the fact that the equations can be solved explicitly for $\delta = 0$. A computation with `Mathematica` gives the following expanded form of Equation (4.56), up to higher-order terms in (w_0, λ, δ) :

$$(4.58) \quad w_0 + 1 - (4 + 3w_0)\lambda \ln \lambda + \frac{1}{288}(1 + w_0)\delta^8 \ln \lambda = 0.$$

Equation (4.58) again contains logarithmic terms due to resonance between the eigenvalues -1 , 0 (double), and 1 of the linearization of Equation (4.52) about the steady state at $(0, -1, -1, 0)$ in chart κ_1 . Solving Equation (4.58) for w_0 gives

$$(4.59) \quad w_0 = -1 + \lambda \ln \lambda + C(\delta)\lambda + \mathcal{O}[\lambda^2(\ln \lambda)^2]$$

with $C(\delta) = \mathcal{O}(\delta^8)$, which is regular in δ , as expected. We note that, for $\lambda = 0$, (4.58) reduces to the trivial equation $w_0 + 1 = 0$, which is solved by $w_0 = -1$, independently of δ . The resulting singular solutions correspond to type II-solutions, which are shown as the part of the green curve in the blown-up bifurcation diagram in Figure 10 that corresponds to $\bar{\varepsilon}$ small. In line with these observations, Equation (4.58) is identical to Equation (4.43) up to terms of order $\mathcal{O}(\delta^2\lambda)$ after the rescaling of w in (2.6). For $\delta = 0$ and $\lambda > 0$, on the other hand, we match with the branch obtained in the part of region \mathcal{R}_3 that corresponds to $\lambda \geq \tilde{\lambda}$.

The results obtained in the above two subregions prove the existence and uniqueness of a curve of solutions to the boundary value problem (2.8)–(2.9) in \mathcal{R}_3 , as stated in Proposition 4.20. It remains to consider the overlap between regions \mathcal{R}_3 and \mathcal{R}_2 : in (λ, δ) -space, \mathcal{R}_3 corresponds to

$$(4.60) \quad [0, 1] \times \left[0, \frac{1}{\sqrt{\lambda_3}}\right] \setminus [0, \varepsilon\lambda_3] \times \left[\frac{1}{\sqrt{\lambda_2}}, \frac{1}{\sqrt{\lambda_3}}\right],$$

while \mathcal{R}_2 covers the area

$$(4.61) \quad [0, \varepsilon\lambda_2] \times \left[\frac{1}{\sqrt{\lambda_2}}, \delta_1\right],$$

where $\delta_1 < \frac{2}{\sqrt{3}}$ is defined in [Proposition 4.5](#). Hence, in (λ, δ) -space, regions \mathcal{R}_3 and \mathcal{R}_2 overlap in the rectangle

$$(4.62) \quad [\varepsilon\lambda_3, \varepsilon\lambda_2] \times \left[\frac{1}{\sqrt{\lambda_2}}, \frac{1}{\sqrt{\lambda_3}} \right],$$

see [Figure 22](#), which is the area where the transition between the two regions occurs. This concludes the proof of [Proposition 4.20](#). \square

[Theorem 1.3](#) is hence proven.

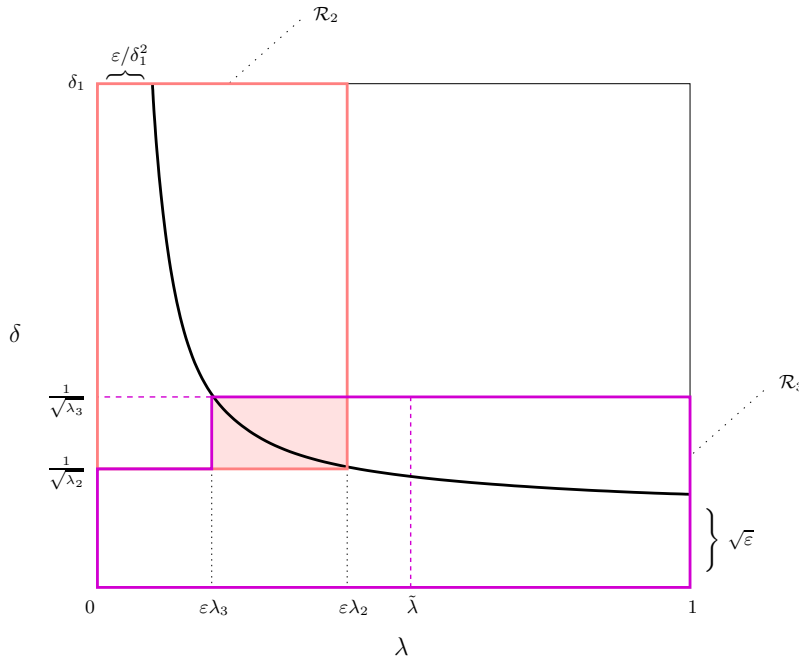


FIGURE 22. Regions \mathcal{R}_2 (pink) and \mathcal{R}_3 (magenta) in (λ, δ) -parameter space; cf. (4.61) and (4.60), respectively. The dashed vertical magenta line at $\lambda = \bar{\lambda}$ delimits the two subregions considered in the proof of [Proposition 4.20](#). The dashed horizontal magenta line at $\delta = \frac{1}{\sqrt{\lambda_3}}$ indicates that the argument employed in the second part of the proof of [Proposition 4.20](#) is valid in the entire rectangle defined in (4.57), where we note that region \mathcal{R}_3 excludes the rectangle $[0, \varepsilon\lambda_3] \times [\frac{1}{\sqrt{\lambda_2}}, \frac{1}{\sqrt{\lambda_3}}]$ by construction; cf. (4.3). Regions \mathcal{R}_2 and \mathcal{R}_3 overlap in the shaded rectangle (light pink) given by (4.62). The black curve corresponds to $\delta^2\lambda = \varepsilon$, for given $0 < \varepsilon \ll 1$.

5. Discussion and Outlook. In this article, we have investigated stationary solutions of a regularized model for Micro-Electro Mechanical Systems (MEMS). In particular, we have unveiled the asymptotics of the bifurcation diagram for solutions of the boundary value problem (2.8)–(2.9), as the regularization parameter ε tends to zero. In that process, we have proven that the new branch of solutions which emerges in the bifurcation diagram of the regularized model derives from an underlying, very degenerate singular structure. Applying tools from dynamical systems theory, in particular, geometric singular perturbation theory and the blow-up method, we have considered separately three principal regions in the bifurcation diagram; cf. [Figure 9](#). We emphasize that our findings are consistent with formal asymptotics and numerical simulations of Lindsay *et al.*; see, in particular, Section 3 of [19] and Section 4 of [20].

One of the most interesting features of the regularized model considered here is the presence of a highly singular saddle-node bifurcation point. While Lindsay *et al.* [19] were able to derive a formal leading-order asymptotic expansion in the regularization parameter at that point, the coefficients therein had remained undetermined thus far. Our approach, on the other hand, allows us to obtain the fold point as the minimum of an appropriately defined bifurcation equation and, hence, to calculate explicitly the coefficients in that expansion. (For completeness, we remark that the coefficient of the leading-order term therein appeared in [19, Section 3] in a different context: $\lambda_{0c} = \frac{m-1}{2(m-2)}$, with $m = 4$; however, that correspondence does not seem to have been noted there.) For verification, a comparison with numerical data obtained with the continuation package AUTO has been performed, showing very good agreement with our analytical results.

Finally, in Lindsay’s work [19], logarithmic terms in ε , as well as fractional powers of ε , occur in the asymptotic expansions of solutions to Equation (1.3) as “switchback” terms that need to be included during matching in order to ensure the consistency of these expansions [22]. Here, we have shown that this somewhat unexpected asymptotics arises naturally due to a resonance phenomenon in one of the coordinate charts, viz. K_1 , after blow-up; see [25] for a more general discussion. Our analysis hence establishes a connection between the geometric approach proposed here and the method of matched asymptotic expansions. That connection has already been observed in various classical singular perturbation problems; examples include Lagerstrom’s model equation for low Reynolds number flow [15, 16, 26] and the generalized Evans function for degenerate shock waves derived in [27].

Our geometric approach to the boundary value problem (2.8)–(2.9) can be extended to the analysis of steady states of the corresponding regularized fourth-order model, which has been studied in [19, 20, 21] both asymptotically and numerically. A future aim is to establish analogous results for that case. Another possible topic for future research is the geometric analysis of Equation (1.3) in higher dimensions, possibly under the simplifying assumption of radial symmetry.

Acknowledgments. AI and PS would like to thank Alan Lindsay for helpful discussions. They would also like to acknowledge the Fonds zur Förderung der wissenschaftlichen Forschung (FWF) for support via the doctoral school “Dissipation and Dispersion in Nonlinear PDEs” (project number W1245). Moreover, AI is grateful to the School of Mathematics at the University of Edinburgh for its hospitality during an extensive research visit.

REFERENCES

- [1] N. DOBLE AND D. WILLIAMS, *The application of MEMS technology for adaptive optics in vision science*, IEEE J. Sel. Top. Quant., 10 (2004), pp. 629–635, <https://doi.org/10.1109/jstqe.2004.829202>.
- [2] E. DOEDEL, *AUTO: a program for the automatic bifurcation analysis of autonomous systems*, in Proceedings of the Tenth Manitoba Conference on Numerical Mathematics and Computing, Vol. I (Winnipeg, Man., 1980), vol. 30, 1981, pp. 265–284.
- [3] F. DUMORTIER, *Techniques in the theory of local bifurcations: blow-up, normal forms, nilpotent bifurcations, singular perturbations*, in Bifurcations and periodic orbits of vector fields (Montreal, PQ, 1992), vol. 408 of NATO Adv. Sci. Inst. Ser. C Math. Phys. Sci., Kluwer Acad. Publ., Dordrecht, 1993, pp. 19–73, https://doi.org/10.1007/978-94-015-8238-4_2.
- [4] F. DUMORTIER AND R. ROUSSARIE, *Canard cycles and center manifolds*, Mem. Amer. Math. Soc., 121 (1996), pp. x+100, <https://doi.org/10.1090/memo/0577>.
- [5] N. FENICHEL, *Geometric singular perturbation theory for ordinary differential equations*, J. Differential Equations, 31 (1979), pp. 53–98, [https://doi.org/10.1016/0022-0396\(79\)90152-9](https://doi.org/10.1016/0022-0396(79)90152-9).

- [6] Y. GUO, Z. PAN, AND M. WARD, *Touchdown and pull-in voltage behavior of a MEMS device with varying dielectric properties*, SIAM J. Appl. Math., 66 (2005), pp. 309–338, <https://doi.org/10.1137/040613391>.
- [7] A. IUORIO, *Geometric analysis of multi-scale solutions in regularized models of microstructures and touchdown phenomena in MEMS*, PhD thesis, Vienna University of Technology, 2018.
- [8] B. IVERSON AND S. GARIMELLA, *Recent advances in microscale pumping technologies: a review and evaluation*, Microfluidics Nanofluidics, 5 (2008), pp. 145–174, <https://doi.org/10.1007/s10404-008-0266-8>.
- [9] C. JONES, *Geometric singular perturbation theory*, in Dynamical systems (Montecatini Terme, 1994), vol. 1609 of Lecture Notes in Math., Springer-Verlag, Berlin, 1995, pp. 44–118, <https://doi.org/10.1007/BFb0095239>.
- [10] C. JONES, T. KAPER, AND N. KOPELL, *Tracking invariant manifolds up to exponentially small errors*, SIAM J. Math. Anal., 27 (1996), pp. 558–577, <https://doi.org/10.1137/s003614109325966x>.
- [11] C. JONES AND N. KOPELL, *Tracking invariant manifolds with differential forms in singularly perturbed systems*, J. Differential Equations, 108 (1994), pp. 64–88, <https://doi.org/10.1006/jdeq.1994.1025>.
- [12] M. KRUPA AND P. SZMOLYAN, *Extending geometric singular perturbation theory to nonhyperbolic points—fold and canard points in two dimensions*, SIAM J. Math. Anal., 33 (2001), pp. 286–314, <https://doi.org/10.1137/s0036141099360919>.
- [13] M. KRUPA AND P. SZMOLYAN, *Geometric analysis of the singularly perturbed planar fold*, in Multiple-time-scale dynamical systems (Minneapolis, MN, 1997), vol. 122 of IMA Vol. Math. Appl., Springer, New York, 2001, pp. 89–116, https://doi.org/10.1007/978-1-4613-0117-2_4.
- [14] C. KUEHN, *Multiple time scale dynamics*, vol. 191 of Applied Mathematical Sciences, Springer, Cham, 2015, <https://doi.org/10.1007/978-3-319-12316-5>.
- [15] P. LAGERSTROM AND D. REINELT, *Note on logarithmic switchback terms in regular and singular perturbation expansions*, SIAM J. Appl. Math., 44 (1984), pp. 451–462, <https://doi.org/10.1137/0144030>.
- [16] P. A. LAGERSTROM, *Matched asymptotic expansions. Ideas and techniques*, vol. 76 of Applied Mathematical Sciences, Springer-Verlag, New York, 1988, <https://doi.org/10.1007/978-1-4757-1990-1>.
- [17] F. LIN AND Y. YANG, *Nonlinear non-local elliptic equation modelling electrostatic actuation*, Proc. R. Soc. Lond. Ser. A Math. Phys. Eng. Sci., 463 (2007), pp. 1323–1337, <https://doi.org/10.1098/rspa.2007.1816>.
- [18] A. LINDSAY AND J. LEGA, *Multiple quenching solutions of a fourth order parabolic PDE with a singular nonlinearity modeling a MEMS capacitor*, SIAM J. Appl. Math., 72 (2012), pp. 935–958, <https://doi.org/10.1137/110832550>.
- [19] A. LINDSAY, J. LEGA, AND K. GLASNER, *Regularized model of post-touchdown configurations in electrostatic MEMS: Equilibrium analysis*, Phys. D, 280 (2014), pp. 95–108, <https://doi.org/10.1016/j.physd.2014.04.007>.
- [20] A. E. LINDSAY, *Regularized model of post-touchdown configurations in electrostatic MEMS: bistability analysis*, J. Engrg. Math., 99 (2016), pp. 65–77, <https://doi.org/10.1007/s10665-015-9820-z>.
- [21] A. E. LINDSAY, J. LEGA, AND K. B. GLASNER, *Regularized model of post-touchdown configurations in electrostatic MEMS: interface dynamics*, IMA J. Appl. Math., 80 (2015), pp. 1635–1663, <https://doi.org/10.1093/imamat/hxv011>.
- [22] A. E. LINDSAY AND M. J. WARD, *Asymptotics of some nonlinear eigenvalue problems modelling a MEMS capacitor. Part II: multiple solutions and singular asymptotics*, European J. Appl. Math., 22 (2011), pp. 83–123, <https://doi.org/10.1017/S0956792510000318>.
- [23] J. PELESKO, *Mathematical modeling of electrostatic MEMS with tailored dielectric properties*, SIAM J. Appl. Math., 62 (2002), pp. 888–908, <https://doi.org/10.1137/s0036139900381079>.
- [24] J. A. PELESKO AND D. H. BERNSTEIN, *Modeling MEMS and NEMS*, Chapman & Hall/CRC, Boca Raton, FL, 2003.
- [25] N. POPOVIĆ, *A geometric analysis of logarithmic switchback phenomena*, in HAMSAs 2004: Proceedings of the International Workshop on Hysteresis and Multi-Scale Asymptotics (Cork, Ireland, 2004), vol. 22, 2005, pp. 164–173, <https://doi.org/10.1088/1742-6596/22/1/011>.
- [26] N. POPOVIĆ AND P. SZMOLYAN, *A geometric analysis of the Lagerstrom model problem*, J. Differential Equations, 199 (2004), pp. 290–325, <https://doi.org/10.1016/j.jde.2003.08.004>.
- [27] B. SANDSTEDTE AND A. SCHEEL, *Evans function and blow-up methods in critical eigenvalue problems*, Discrete Contin. Dyn. Syst., 10 (2004), pp. 941–964, <https://doi.org/10.3934/>

- [dcds.2004.10.941](#).
- [28] N. TSAI AND C. SUE, *Review of MEMS-based drug delivery and dosing systems*, Sens. Actuators A Phys., 134 (2007), pp. 555–564, <https://doi.org/10.1016/j.sna.2006.06.014>.
- [29] B. WATSON, J. FRIEND, AND L. YEO, *Piezoelectric ultrasonic micro/milli-scale actuators*, Sens. Actuators A Phys., 152 (2009), pp. 219–233, <https://doi.org/10.1016/j.sna.2009.04.001>.
- [30] S. WIGGINS, *Introduction to applied nonlinear dynamical systems and chaos*, vol. 2 of Texts in Applied Mathematics, Springer-Verlag, New York, second ed., 2003.